

CABRILLO 1.0: Acoustic, elastic and poroelastic finite difference modelling

Peter Gerstoft
Marine Physical Laboratory
University of California at San Diego, La Jolla CA-92093-0701 USA

August 31, 2002

Contents

1	Introduction	3
2	Installing CABRILLO	5
2.1	CABRILLO directory	5
2.2	Loading CABRILLO files	5
2.3	CABRILLO platforms	6
2.4	Building CABRILLO	6
3	Grid generation	7
3.1	Example of acoustic grid generation file	9
3.2	Example of elastic poroelastic grid generation file	10
4	Running the finite difference codes	11
4.1	Format of the source.time file	13

4.2	Output files	13
4.3	Plotting codes	15
4.4	Example of acoustic run file *.par	15
5	Examples	17
5.1	Propagation across one interface	17
5.1.1	Acoustic media	17
5.1.2	Elastic media	17
5.1.3	Poroelastic media	19
5.2	Poroelastic media, benchmarking	24
5.3	Sloping bottom	24
5.4	Time reverse mirror	31
5.4.1	One interface	31
5.4.2	High frequency, acoustic case	31
5.4.3	Elastic media, high frequency	34
5.5	Tommeliten	41
A	APPENDIX A: Background	45
A.1	Acoustic media	45
A.2	Elastic media	45
A.3	Poroelastic media	45
A.3.1	Material parameters	46
A.3.2	Zero frequency limit of P and S wave	47
A.3.3	The equations	47
A.3.4	Fluid media	48

A.3.5 Elastic media	48
A.4 Fourier spectral method	49
A.5 Time derivative	49
A.6 Sampling conditions	50
A.7 Boundary conditions	51
A.8 Number of FFT blocks	52
A.9 Source function	52
B APPENDIX B: Gas Bubbles in acoustic or elastic media	54

Abstract

Cabrillo is a staggered Pseudo-spectral finite difference code for acoustic elastic and poroelastic media. The advantage of a FD approach is that a geometric complicated media can be modeled. Staggered grids are advantageous as it provides more accuracy and can handle larger velocity and density contrasts than using a classic grid. In a Pseudo-spectral method the spatial derivatives are evaluated by a wavenumber multiplication in the wavenumber domain. The advantage of this approach are stability and reduction in memory and the number of computations required to obtain a given accuracy. Usually FD codes cannot handle attenuation. But, using Biot theory it is also possible to incorporate attenuation into the media by increasing the viscosity.

Much care has gone into obtaining a fast and reliable code. The kernel of the code is based on a code from University of Dallas [2, 1]. The Temperton Fourier transform is used as the FFT (obtained from the University of Hamburg). This allows the number of grid points to be any combination of prime factors up to 11.

CABRILLO was the explorer that discovered beautiful San Diego, where the code has been developed.

1 Introduction

The time domain wave equation is here solved directly by the Finite difference method—that is the so-called Time Domain Finite Difference (TDFD) solution. This is in contrast to many other methods that is based on the frequency domain solution of the Helmholtz solution. For the TDFD the solution is the time evolution of the field across the spatial grid. Thus the solution is presented as either timeseries at selected points in space or as snapshots at selected points in time.

The Fourier spectral method is used for solving the wave equation. It now seems clear that a low order FD method is not as computational efficient as high order (e.g. 8th order) FD or a spectral method[3]. Which of the two latter methods is preferable probably depends on the geometry of the problem.

Spectral finite difference methods has been used extensively in the seismic exploration literature[4, 5, 6, 7, 8, 9]. It has also been applied to Biot media [1, 2]. But it has not yet been applied in ocean acoustics, where other finite difference methods has been used sparsely [11, 12, 13].

Demand for computer resources by FD methods has long been of major concern. Concerning memory Fourier spectral methods requires a factor 5 less modes per wavelength. This implies that spectral methods are about a decade more memory efficient than classical FD for a 2D problem. For 3D this factor is about two decades.

Concerning CPU times, faster computers has reduced this problem. The initial acoustic modeling of each problem in this example has been done in less than a minute. For a typical problem of a 100×100 grid with 1000 time samples the Cpu-time on a Sun Solaris workstation is 70 s for acoustic media, 175 s for elastic and 350 s for poroelastic. A doubling of the grid points in one grid dimension increases the CPU time by a factor 2 for small grid (less than 500 points) and a factor 2.5 for large grid. A doubling of the time samples doubles the CPU time.

2 Installing CABRILLO

2.1 CABRILLO directory

The CABRILLO home directory is defined on UNIX systems by the following command in your .login:

```
setenv CABRILLO your-CABRILLO-root-directory
```

This could e.g. be `$HOME/cabrillo`. For execution of CABRILLO you must include the scripts and executables in your search path, i.e. `CABRILLO/bin`. The following line should be inserted in your .login:

```
set path = ($CABRILLO/bin $path)
```

In order to execute the MATLAB files the `($CABRILLO/matlab` directory should be in your `matlab-path`.

2.2 Loading CABRILLO files

For users running UNIX, the whole directory tree is provided in a compressed **tar** file with the name

```
cabrillo.tar.Z
```

Place this file in your desired root directory `$HOME` and issue the commands:

```
uncompress cabrillo.tar.Z
```

```
tar xvf cabrillo.tar
```

which will install the directory tree:

<code>\$CABRILLO</code>	CABRILLO root directory
<code>\$CABRILLO/src</code>	Source files for CABRILLO
<code>\$CABRILLO/bin</code>	CABRILLO scripts and destination of executables
<code>\$CABRILLO/examples</code>	Examples for running CABRILLO
<code>\$CABRILLO/doc</code>	This document in L ^A T _E X and Postscript format
<code>\$CABRILLO/matlab</code>	Some MATLAB files

2.3 CABRILLO platforms

CABRILLO has been developed under SunOS 5.5. For addressing some variables pointers are used. This feature will give problems on some systems, as for example SGI and Cray. The pointers are not very important for the execution time and the use of pointers will be abolished in a later version.

Under SunOS it is possible to use the highest level of optimization. This is quite important for obtaining fast run times.

2.4 Building CABRILLO

Set your default directory to `$CABRILLO/src` and edit the **Makefile**. Set the definition of the Fortran compiler and your desired directories for libraries and executables (typically `$CABRILLO/bin`).

You should decide which forward models you would like to compile. This can easily be selected by commenting them in the “all line” in the **Makefile**. Also the Fortran compiler options should be modified in the **Makefile** in `src` directory. For production runs, it is advisable to compile with a high level of optimization and without array checking.

After performing the changes, compile and link by issuing the command:

```
make all
```

which will generate all CABRILLO modules.

If the default parameter settings are too large or too small to run a given problem, the parameters may be altered in the parameter include file **param.h**. Sometimes the parameters controlling the forward modeling routines should also be changed.

Input parameter	Description
Block I: TITLE (1 line)	
TITLE	Title of run
Block II: FD- PARAMETERS (3 lines)	
nx nz	number of steps in x, z for <i>grid</i> code
dx dz	discretization in x, z (half grid spacing!)
imedia igeo	Biot(3), elastic(2) or acoustic(1) media igeo: specify geometry for each physical variable (=0) or only the first (=1)
Block III: Name of Physical parameters ($N_z + 2$ lines)	
parameter-name	dummy
Block IV: Geometry of Physical parameters ($N_z + 2$ lines)	
$Nx \quad Nz$ $x_1 \dots x_{Nx}$ $z_{11} \dots z_{1Nx}$ \vdots $z_{Nz1} \dots z_{NzNx}$	The x coordinates along the grid generation The z coordinates
Block V: Physical parameters	
$c_{11} \dots c_{1Nx}$ \vdots $c_{Nz1} \dots c_{NzNx}$	This should be specified for each physical parameter

Table 1: GRID input file structure `filename.grid` (all units are SI units). Block III–V should be repeated for each physical parameter. No blank lines is allowed in the file.

3 Grid generation

A central part of a Finite difference package is a grid generation code. At present, there is one grid generation code. It is executed by typing

```
grid filename
```

It reads from `filename.grid` and writes the grid to `filename.phy`. The `filename.phy` can then be read by the FD code. The `filename.grid` should have the structure as indicated in Table 1. First some central FD parameters is specified. It should here be noted that the number of grid points and the spacing refers to the full grid, whereas in the FD codes it refers to the staggered grid size(i.e. $Nx_{FD} = Nx_{GRID}/2$ and $dx_{FD} = 2 * dx_{GRID}$). One block is a geometric specification of each physical parameter. Because a Fast Fourier transform is used the number of grid points for the FD codes should be multiples of 2, 3, 5, 7 or 11. The geometry of the problem can be specified for each block (*igeo* = 0) or only for the first block (*igeo* = 1).

The physical parameter $c_{11} \dots c_{NzNx}$ is specified in a set of control points from (x_1, z_{11}) at the upper left corner to (x_{Nx}, z_{NzNx}) at the lower right corner. Note, that the x -coordinate has one

index whereas the z -coordinate has two. Using linear interpolation in both directions the value of the given parameter at the FD grid is interpolated over the entire grid.

The grid is generated starting from the (x_1, z_{11}) control point. It is required that the entire grid can be contained with the control points (the last control point might be outside the grid; then the value for the last grid point. The first control point does not need to start at $(0, 0)$, but the grid is translated so that the FD-grid always start at $(0, 0)$.

Based on the P-wave velocities, the maximum time step and the maximum center frequency of the wavelet is computed using the sampling rules in Sect. A.6. Not, that in order to obtain correct sampling of the field these rules should be followed for all propagating waves (Interface waves, S-waves, P-I and P-II waves).

This file has the same structure for acoustic, elastic or poroelastic media, but different number of parameter blocks must be specified (2 blocks for acoustic, 3 blocks for elastic and 11 for poroelastic media. The type of media is specified by the `imedia` parameter [Biot(3), elastic(2) or acoustic(1) media].

for **acoustic** media the blocks are:

P-wave velocity (m/s)
density (kg/m^3)

for **elastic** media the blocks are:

P-wave velocity (m/s)
density (kg/m^3)
S-wave velocity (m/s)

for **poroelastic** media the blocks are:

P-wave velocity of saturated rock, v_p (m/s)
S-wave velocity of saturated rock, v_s (m/s)
Bulk modulus of fluid, k_f (Pa)
Bulk modulus of solid grains, k_g (Pa)
Bulk modulus of dry porous frame, k_b (Pa)
Density of saturated rock, ρ_f (kg/m^3)
Density of fluid, ρ_f (kg/m^3)
Porosity of the rock, ϕ ()
Viscosity of the fluid, η (Pa s)
Permeability of the rock, p_k (m^2)
Added mass, a ()

3.1 Example of acoustic grid generation file

This example computes the material parameters on the grid in preparation to compute the response as in Fig. 16. The example is for a dimension of 16x16 cm and the half grid spacing is 0.2 mm. That gives 800 grid points in total in each direction. Because the density is constant we have chosen to specify the geometry for each of the material parameters, $i_{geo} = 0$. In order to have a sharp contrast two control points are specified very close together (i.e., from 0.04 to 0.041, and from 0.08 to 0.081). The starting coordinates is $(-0.02, -0.02)$, the grid will then be translated so that it starts at $(0, 0)$ and when executing the FD codes all geometric parameters (source and receivers) should be specified from a grid starting at $(0, 0)$.

```
Acoustic example.
800 800          ! number of grid points
.0002 .0002      ! half grid spacing
1 0             ! acoustic (1) media; geometry for each physical parameter (0)
sound speed****
6 10            ! number of x and z input
-0.02 0.04 0.041 0.08 0.081 0.16 ! x-coordinates
-0.02 -0.02 -0.02 -0.02 -0.02 -0.02 ! z-coordinates
0.02 0.02 0.02 0.02 0.02 0.02 ! z2
0.021 0.021 0.021 0.021 0.021 0.021 ! z3
0.04 0.04 0.04 0.04 0.04 0.04 ! z4
0.041 0.041 0.041 0.041 0.041 0.041 ! z5
0.06 0.06 0.06 0.06 0.06 0.06 ! z6
0.061 0.061 0.061 0.061 0.061 0.061 ! z7
0.08 0.08 0.08 0.08 0.08 0.08 ! z8
0.081 0.081 0.081 0.081 0.081 0.081 ! z9
0.16 0.16 0.16 0.16 0.16 0.16 ! z10
1500 1500 3000 3000 3000 3000 ! c1
1500 1500 3000 3000 3000 3000 ! c2
1500 1500 1500 1500 3000 3000 ! c3
1500 1500 1500 1500 3000 3000 ! c4
1500 1500 3000 3000 3000 3000 ! c5
1500 1500 3000 3000 3000 3000 ! c6
1500 1500 1500 1500 3000 3000 ! c7
1500 1500 1500 1500 3000 3000 ! c8
1500 1500 3000 3000 3000 3000 ! c9
1500 1500 3000 3000 3000 3000 ! c10
density ****
2 2            ! number of x and z input
-0.02 0.16     ! x-coordinates
-0.02 -0.02    ! z-coordinates
1000 1000      ! density 1
1000 1000      ! density 2
```

3.2 Example of elastic poroelastic grid generation file

These have similar format as the acoustic example. They are provided in the example directory.

Input parameter	Description
Block I: TITLE (1 line)	
TITLE	Title of run
Block II: OPTIONS (1 line)	
A B C ...	Output and computational options.
Block III: FD-parameters (4 lines)	
nx nz nt	number of steps in x, z and t for <i>FD</i> code
dx dz dt fc	discretization in x, z and t, center frequency
lt qt	number of sponge points, tapering factor
nprint	printing information for every nprint time step
Block IV: Source (Nsource+1 lines)	
Nsource	number of sources
sx sz	source coordinates
...	one line for each source
Block V: Seismograms (2 lines)	
rmin rmax delta_r	Range sampled between rmin and rmax at delta_r
dmin dmax delta_d	Depth sampled between dmin and dmax at delta_d
Block VI: Snapshots (1 lines)	
Tstart Tstop delta_t	starting, stopping and delta time for snapshots

Table 2: FD input file structure, `filename.par` (all units are SI).

4 Running the finite difference codes

CABRILLO consists of three codes corresponding to acoustic, elastic or poroelastic media. They are executed by typing respectively

`acou filename`

`ela filename`

`biot filename`

The `filename` refers to the file name without the file extension. It will read the environment from the `filename.phy` file, which will contain different parameters depending on the medium type. Usually, it has been generated using the grid generation code, Sect. 3. The system file `filename.par` whose format is shown in Table 2, does not contain any media specific parameters and can be used for all media types.

Block II Options

S or **S1** must be specified for generating snapshots.

G A non-staggered grid is used. The secondary grids is collapsed to one grid, i.e. only the black grid in Fig. 26, even though some of the material parameters might have been

generated on the secondary grid. This can be used to check the advantage of using a staggered grid.

- F** Free surface. This option put a medium with zero impedance above the free surface, and thus there is no need to specify this layer in the grid input file. The first line for the medium should therefore be the physical layer.
- T** A time series is supplied for each source. The filename should be `source.time`, see sect. 4.1. This does not work for Biot media. The default is to use a synthetically generated Ricker wavelet, see sect. A.9.
- S** Snapshots is plotted for the whole grid. Thus, waves close to the edge will experience attenuation due to tapering of the grid.
- S1** Snapshots is plotted only for the unattenuated part of the grid. Here, no artificial attenuation of the waves is seen.
- Q** Debugging. More information is written out.

Block III: FD-parameters:

The finite difference grid is specified in terms of the number of grid points (`nx`, `nz`) and their spacing (`dx`, `dz`). Because a Fast Fourier transform is used the number of grid points for the FD codes should be multiples of 2, 3, 5, 7 or 11. The number of grid points and spacing specifies the whole grid including sponge layer. The right and left sponge layer is simply defined by using that part of the grid (`lt` columns in left and right side). The top sponge layer is defined by duplicating the material properties in the first row in the whole sponge layer (`lt` rows). In order to keep the number of rows `nz` constant `lt` rows are deleted from the bottom of the grid. Now, the bottom sponge layer is the lower (`lt` rows).

Concerning the sponge layer, good values from the literature are (`lt`, `qt`)= (20, 0.015) or (`lt`, `qt`)= (24, 0.0145). I have good experiences with lower values of the attenuation, (`lt`, `qt`)= (30, 0.010) and (`lt`, `qt`)= (40, 0.006). Note, that if a smaller time step is used the waves will get more attenuated as they transverse the sponge layer and thus a lower value of `qt` is recommended. A problem with the sponge layer is that they can give reflections with a low frequency content.

The code stops with error warnings if there is sources or receiver in the sponge layer. Due care must be exercised when selecting the discretization in space and time `dx,dz,dt`. Some advice on this is provided in Sect. A.6.

The variable `iprint` print information to the screen every `iprint` timestep.

Block IV: Sources:

The source is a Ricker wavelet with centre frequency `fc`, see Sect. A.9. `Nsource` sources are used. For each source the coordinate (`sx`, `sz`) is specified.

Block V: Seismograms:

The seismograms are specified for a grid of receivers. In range the receiver grid is from `rmin` to `rmax` with increment `delta_r` and in depth from `dmin` to `dmax` with increment `delta_d`.

Block VI: Snapshots:

Snapshots are output from `Tstart` to `Tstop` with increment `delta_t` .

4.1 Format of the `source.time` file

With this option a time series is read for each source used in code. This could for example be used with a time reverse mirror example. It could also be used to input time series generated from another code. An example of this could be to use a normal mode code for long range propagation and then let the geometrically more flexible FD code handle the interaction towards the shore. This is only available for the acoustic or elastic code.

For acoustic media the format is:

```
READ(20,*) Nsource, Ntime
do itime=1,Ntime
    READ(20,*)itime
    READ(20,*)(stime(ix),ix=1,Nsource) ! pressure component
enddo
```

For elastic media the format is:

```
READ(20,*) Nsource, Ntime, 2
do itime=1,Ntime
    READ(20,*)itime
    READ(20,*)(stime(ix),ix=1,Nsource) ! for the horizontal source component
    READ(20,*)(stime(ix),ix=1,Nsource) ! for the vertical source component
enddo
```

where `Nsource` is the number of sources and `Ntime` is number of time steps where the source signal is non-zero. The timestep `dt` is assumed to be the same as that specified in Block III of the `filename.par` file.

The matlab function `writesource.m` writes the timeseries in this format for an acoustic media.

4.2 Output files

The code produces two types of output. Snapshot files that shows the field at one point in time and timeseries that shows the variation in time.

The snapshot files can be read with the matlab file `readsnap.m` and a template for plotting is `plotsnap.m`. The times at which snapshots are provided are given by Block VI and the points in space are those specified by the grid, i.e. a spacing dx and dz .

The timeseries file can be read with the matlab file `readseis.m` and a template for plotting is `plotseis.m`. The sampling in space of the timeseries are given by Block V and the sampling in time is determined by dt .

For the **acoustic** code the following files are output:

fort.51 snapshots of pressure

fort.61 timeseries of pressure

For the **elastic** code:

fort.51 snapshots of horizontal displacements

fort.52 snapshots of vertical displacements

fort.53 snapshots of pressure

fort.54 snapshots of shear stress

fort.61 timeseries of horizontal displacements

fort.62 timeseries of vertical displacements

For the **poroelastic** code:

fort.51 snapshots of horizontal displacements of solid frame

fort.52 snapshots of vertical displacements of solid frame

fort.53 snapshots of relative horizontal displacements of fluid

fort.54 snapshots of relative vertical displacements of fluid

fort.61 timeseries of horizontal displacements of solid frame

fort.62 timeseries of vertical displacements of solid frame

fort.63 timeseries of relative horizontal displacements of fluid

fort.64 timeseries of relative vertical displacements of fluid

Format of snapshot file

The snapshot file is written in the following format:

```
write(51,*)nxsnap,nzsnap,itsnap,dx,dz,nx_low,lt,xs(1),zs(1)
do insnap=1,itsnap
  write(51,*) issnap,t,insnap,insnap
  do 505 ix=nx_low,nx_up
    write(51,*)(pressure(ix,iz),iz=nz_low,nz_up)
  enddo
enddo
```

Format of timeseries file

The timeseries file is written in the following format:

```

write(61,*)nrec,ndep,nt,DelRec,DelDep,dt
write(61,*)(xr(i),i=1,nrec)
write(61,*)(zr(i),i=1,ndep)
do it=1,n_TimeStep
    write(61,*)((pressure(ixr(i),izr(j),it),i=1,nrec),j=1,ndep)
enddo

```

4.3 Plotting codes

All output from CABRILLO is plotted using `matlab`.

snapshots:

Snapshots is plotted using `plotsnap.m` in `$CABRILLO/matlab`. For a first plot just execute this file and it will show a set of snapshots from file `fort.51` using the `readsnap.m` to read this files. The last frame will show a plot of the P-wave velocity structure, plotted by `plotvel.m` and read from the file `velocity`. This file is generated from the grid code. For a particular example some features should probably be changed, so copy the `plotsnap.m` file from `$CABRILLO/matlab` to your current directory and modify accordingly.

wiggle plots:

Time series at the grid of receivers are plotted using `plotseis.m` in `$CABRILLO/matlab`. It reads the time series from the file `fort.61` using the `readseis.m` to read this files. For a selected column `idep` of receivers it plots a set of vertically stacked seismograms using the function `wiggle.m`. For a selected row `irow` of receivers it plots a set of horizontally stacked seismograms using the function `hwiggle.m`. [A particular `irow` and `ifile` is selected by editing the `snapshot.m` file. It can also time reverse the signal and write it to `source.time`. For a particular example some features should probably be changed, so copy the `plotseis.m` file from `$CABRILLO/matlab` to your current directory and modify accordingly.

4.4 Example of acoustic run file *.par

This file format is similar for acoustic, elastic and poroelastic media. Thus only one example is provided.

This example is a continuation of the grid generation example in Sect. 3.1. Note, that only the primary grid is specified, `nx` and `nz` is now 400 [they were 800 in the grid example] and `dx` and `dz` is now 0.0004 [instead of 0.0002]. The sampling time is 0.02 μ s and 5001 samples are used to a maximum time of 100 μ s. A sponge layer with 30 points and a tapering factor of 0.01 is used. The source is at (0.02 m, 0.03 m), as no external source function is specified a Ricker wavelet with center frequency 0.73 MHz is used. 13 receivers are specified in range from 0.02 m to 0.14 m in steps of 0.01 m and 13 receivers are specified in depth from 0.01 m to 0.13 m

in steps of 0.01 m. 50 snapshots are output from 2 μ s to 100 μ s in steps of 2 μ s.

```
acoustic media
S1                ! options
400 400 5001      ! nx,nz,nt
.0004 .0004 2e-8 0.73e6 ! dx,dz,dt,fc
30 0.010         ! lt,qt
1                ! iprint
1                ! number of sources
0.02 0.03        ! xs,zs
0.02 0.14 0.01   ! receivers: Rmin Rmax Dr
0.01 0.13 0.01   !               Zmin Zmax Dz
2e-6 100e-6 2e-6 ! snapshots: First, Last, delta
```

5 Examples

All the examples discussed in this Section and others are available in the `$CABRILLO/examples` directory.

5.1 Propagation across one interface

5.1.1 Acoustic media

The first example considers an acoustic medium with an interface at 800 m depth. The upper medium has $c_p = 1500$ m/s and the lower medium has an increasing sound speed from left ($c_p = 2000$ m/s) to right ($c_p = 4000$ m/s). This medium is “infinite”, there is no pressure release surface. At the edge of the grid it is surrounded by a sponge layer that absorb the waves as they hit the edge. The source is a Ricker wavelet with a center frequency of 40 Hz and is at 600 m depth, 200 m from the interface. Snapshots of the pressure field for this example is in Fig. 1 along with the environmental model (in lower right corner). All snapshots are plotted on the same color scale, thus the decrease in amplitude is evident. The reflected wave begins at about $t = 0.3$ s. For $t = 0.35 - 0.6$ s it is evident that the lower medium has a higher velocity to the right, as the waves travels faster in that side. For $t = 0.45 - 0.55$ s a headwave can be seen, it is tangent to the reflected arrival and joins the wave in the lower layer.

5.1.2 Elastic media

We here model elastic wave propagation close to a strong interface contrast. The half space has $c_{p1} = 1500$ m/s, $c_{s1} = 500$ m/s, $\rho_1 = 1000$ kg/m³ and the half space has $c_{p2} = 3000$ m/s, $c_{s2} = 1500$ m/s, $\rho_2 = 2000$ kg/m³. In order to excite the interface wave the Ricker source ($f_c = 40$ Hz) is placed 10 m above the interface. It is useful to display different components of the wavefield and snapshots of horizontal (1st row) and vertical (2nd row) displacements, pressure [see Eq. (A10)] (3rd row) and shear stress [see Eq. (A6)] (4th row) are displayed in Fig. 2. The direct wave and the reflected wave in the upper medium collapse to one circular spreading wave in the upper half space. The P-wave propagates faster in the lower medium, as $c_{p1} < c_{p2}$. Note, the change in polarity as the vertical source plane is passed for both horizontal displacements and shear stress. A headwave connecting the bottom layer P-body wave to the P-body wave in the upper layer can easily be seen. There is also a headwave from the body P-wave in the lower layer to the shear wave in lower layer. Finally there is a headwave from the interface wave to the shear body wave in the top layer.

In the pressure display (3rd row in Fig. 2) the propagating shear waves cannot be seen. But the interface waves can be seen as they are a combination of P and S waves. Finally, in the

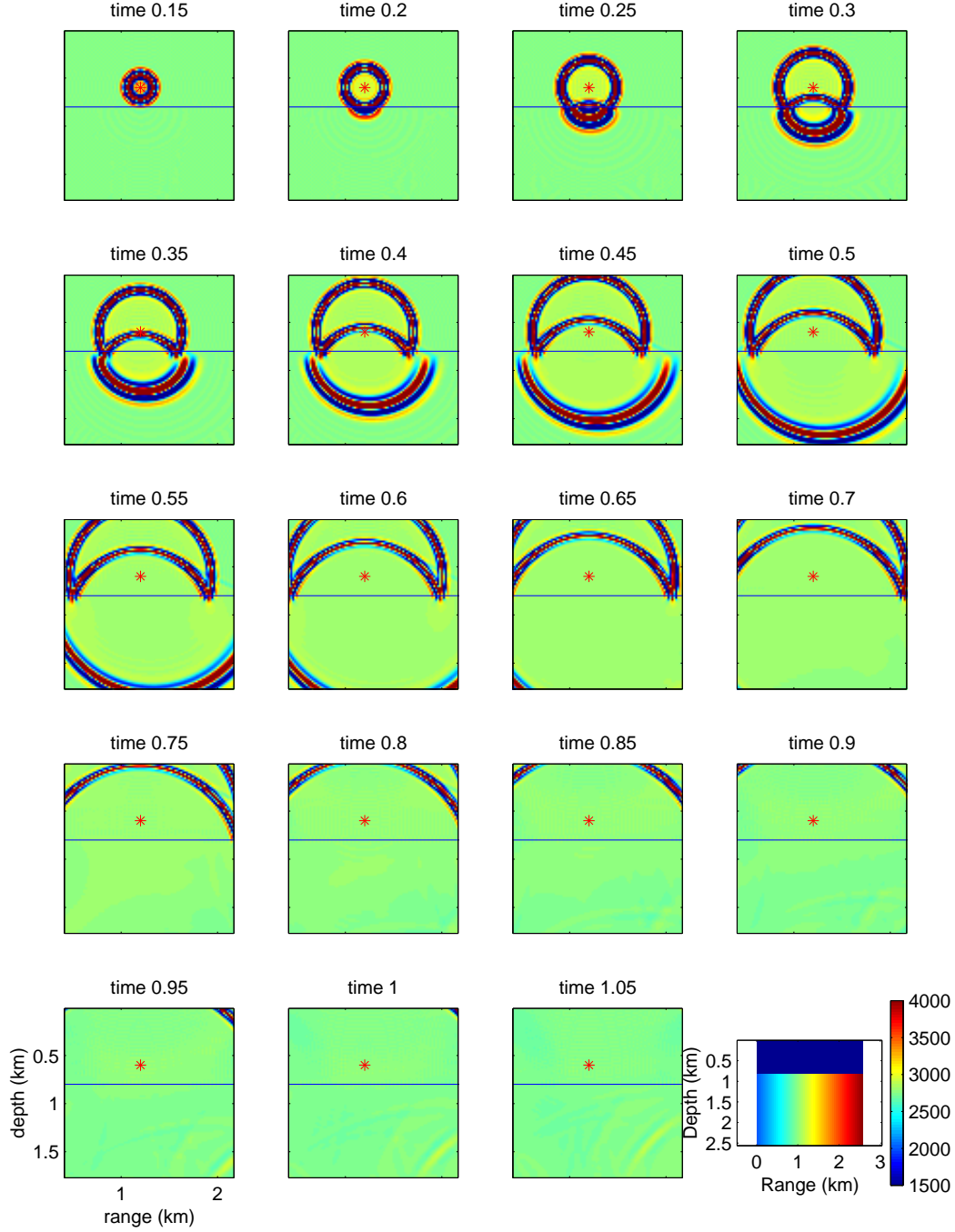


Figure 1: Snapshots of pressure for acoustic propagation across an interface, each panel shows the time evolution of the field. The upper medium has $c_p = 1500$ m/s and the lower medium has an increasing sound speed from left ($c_p = 2000$ m/s) to right ($c_p = 4000$ m/s), see the lower right corner. This medium is “infinite”, but small reflections can be seen from the edge of the grid for later times. [horacu]

Table 3: Material parameters for poroelastic media of sandstone saturated with gas or water. The values stems from [21]

	Gas	Water
	Upper medium	Lower medium
P-wave velocity of saturated rock, v_p (m/s)	1499.6	2204.9
S-wave velocity of saturated rock, v_s (m/s)	992.1	927.8
Bulk modulus of fluid, k_f (GPa)	.022	.400
Bulk modulus of solid grains, k_g (GPa)	35.0	35.0
Bulk modulus of dry porous frame, k_b (GPa)	1.7	1.7
Density of saturated medium, ρ (g/cm ³)	1885	2158
Density of fluid, ρ_f (g/cm ³)	0.0012	1.0
Porosity of the rock, ϕ ()	0.300	0.300
Viscosity of the fluid, η (Pa s)	0	0
Permeability of the rock, p_k (m ²)	1.000E-12	1.000E-12
Added mass, a	2.2	2.2

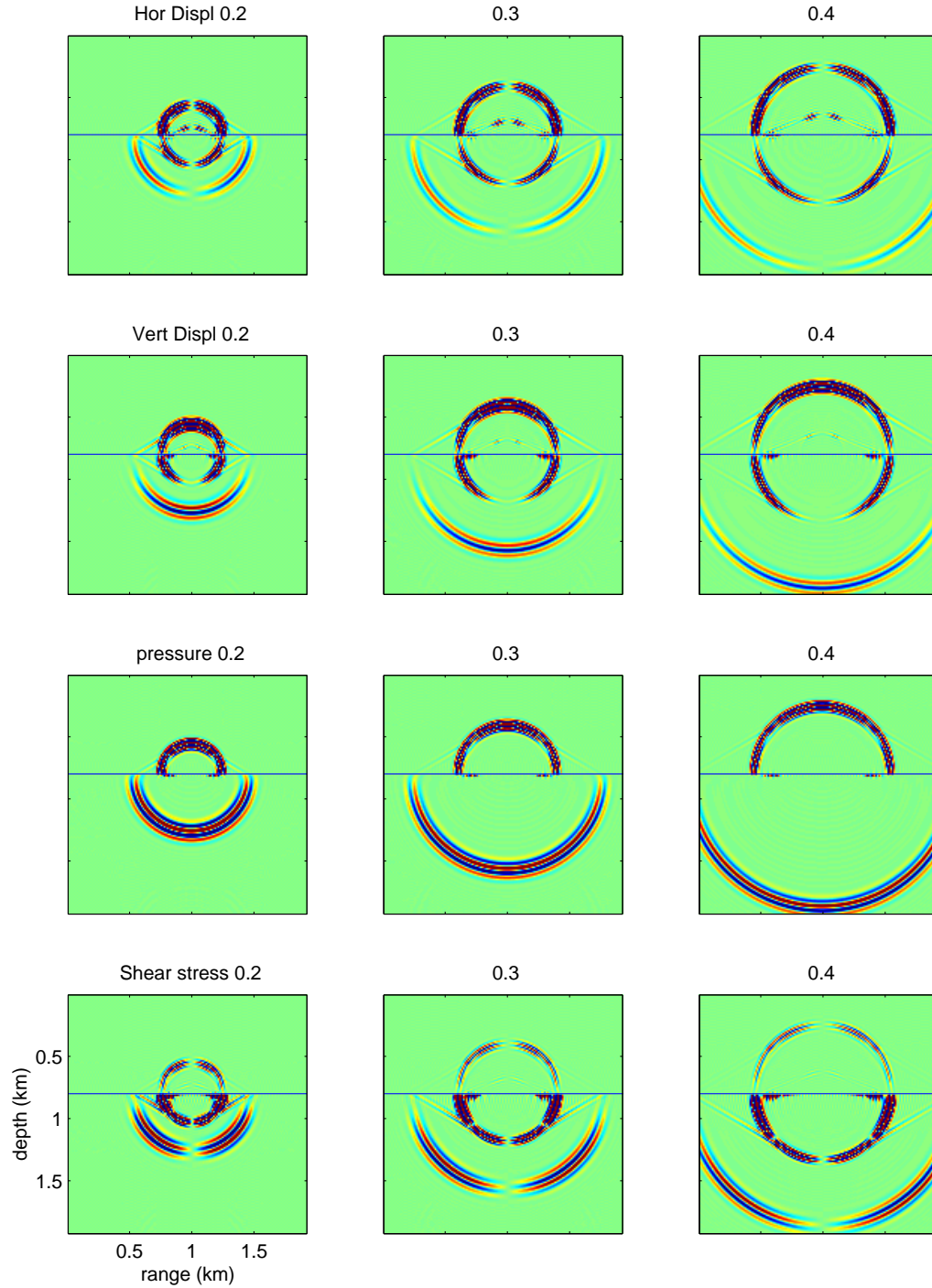
shear stress (4th row in Fig. 2) the interface wave is clearly seen. It propagates with a speed slightly lower than the S-velocity.

5.1.3 Poroelastic media

For examination of the wave field in a poroelastic media the sandstone model used in Refs. [21, 2] is used, see table 3. Based on the equations in the Appendix of Collins *et al.* [14] the frequency dependent velocity and attenuation for each wave type can be found, see Figs. 3 and 4 for a water and gas saturated limestone, respectively. Similar curves was also computed in Ref [21]. Both the P-I and the S-waves vary very slowly with frequency, but the P-II wave depends significantly on frequency. For a frequency of 15 Hz the sound speed is seen to be quite low, about 30 m/s for the water saturated material and close to zero for the gas filled material.

Based on the two poroelastic materials we replicate Fig. 2 of [2], see fig 5. An infinite medium with gas-saturated limestone down to 1 km and water-saturated limestone below. The source is a 15 Hz Ricker wavelet, placed 200 m above the interface. 400× 400 staggered grid point is used with an grid increment of 5 m. The time increment is 0.0004 s and the snapshot is displayed at 0.52 s. There are differences in the reflected energy. This is due to an error in the previous version of the code. Notice as expected, that for vertical incidence there is no shear waves, in Ref. [2] that was not the case.

From top to bottom the following waves can be identified in the top halfspace (it is also easy to detect these waves based on the snapshots in Fig. 6): The direct P-wave, the reflected P-wave, the reflected shear wave (passing through the circular wave), the reflected slow P-wave,



File: /clio1/gerstoft/ld/elas/interface/ ; Date: 04-Jan-1999

Figure 2: Snapshots for elastic propagation across an interface, each vertical column shows the time evolution of the field, while the rows displays Horizontal displacements (1st row), vertical displacements (2nd row), pressure (3rd row) and shear stress (4th row). Notice the interface wave in especially the shear stress displays. CPU time = 200 s. [elaint]

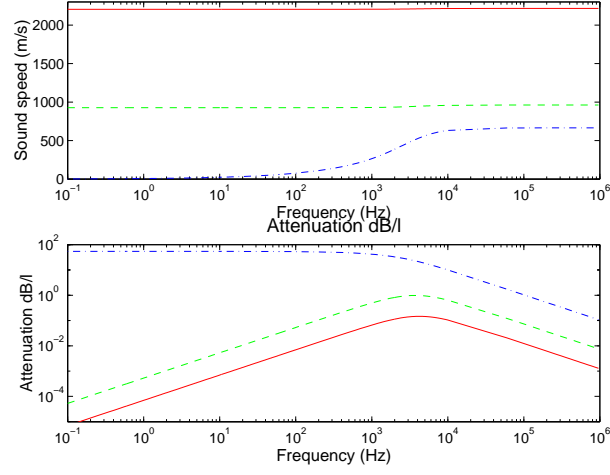


Figure 3: Velocities (top) and attenuation (bottom) for a sandstone filled with water for P-I-wave (full), S-wave(dashed) and P-II wave (dashed-dotted). [**velduttawater**]

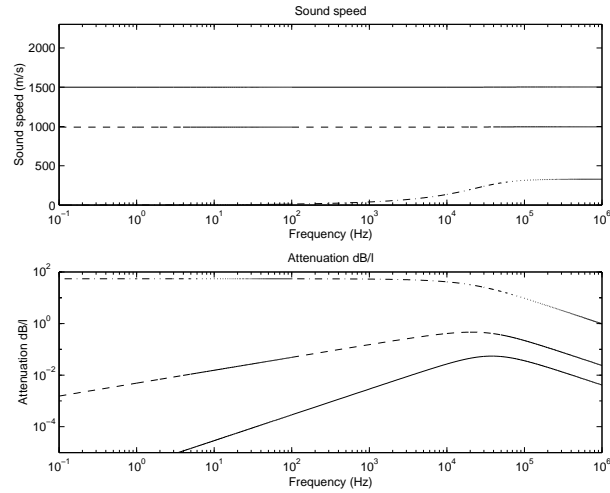


Figure 4: Velocities (top) and attenuation (bottom) for a sandstone filled with gas for P-I-wave (full), S-wave(dashed) and P-II wave (dashed-dotted). [**velduttagas**]

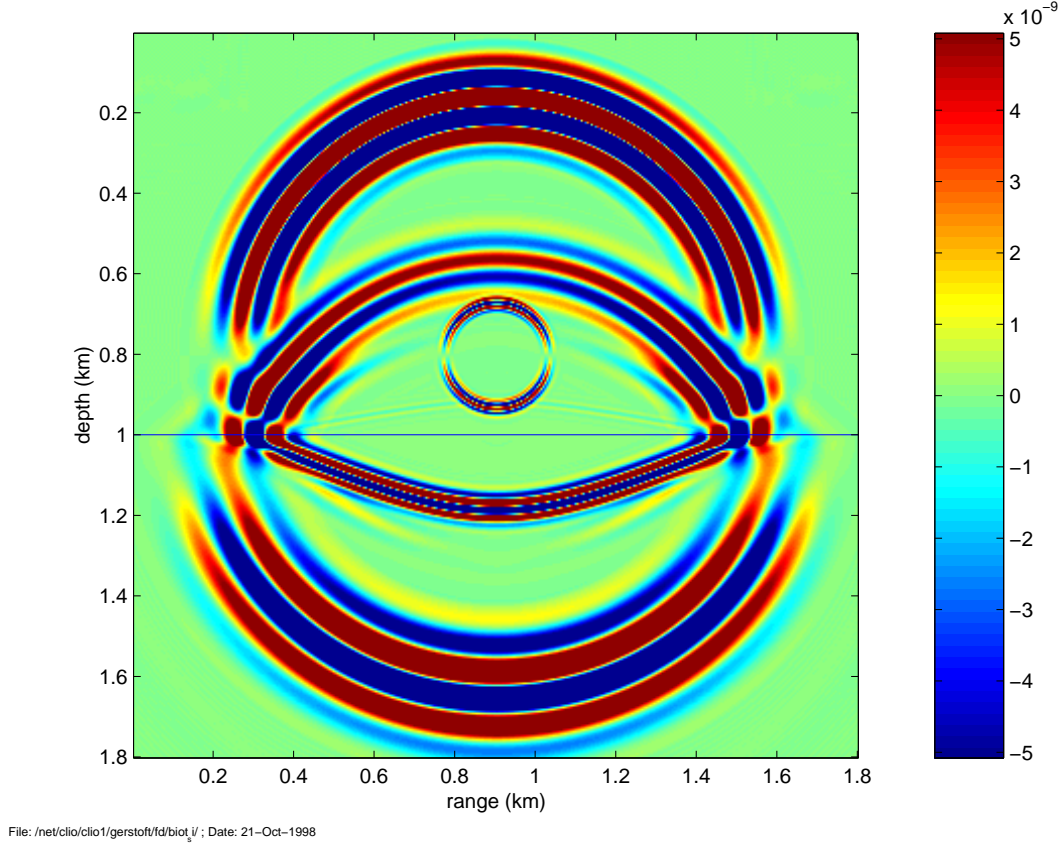


Figure 5: Snapshot at 0.52 s of vertical solid displacements for fluid saturated limestone with gas above the interface at 1 km depth and water below, for the material parameters see ta:mat. Grid size is 400x400 and number of time steps is 1300. The color scale units are arbitrary. CPU time=9000 sec. [dutta]

and finally the circular wave is the direct slow wave. In the bottom halfspace we identify the following transmitted waves from the direct P-wave: the slow P-wave, the S-wave and the P-wave.

The slow circular wave close to the source is attributed to the slow P wave. However, based on two snapshots, the speed of the P-II wave seems to be about 250 m/s. This is in contrast to the sound speeds found above for this frequency (close to zero). This could be due to the fact that the FD-grid does not support so slow waves, as the grid spacing must be less than half a wavelength, see Sect:se:samp. But the grid does support waves with a speed of about $2 \times 5 \text{ m} \times 15 \text{ Hz} = 150 \text{ m/s}$. Decreasing the grid size did not seem to make the apparent sound speed lower (results not shown). The difference in sound speed could also be due to differences in the mathematical model.

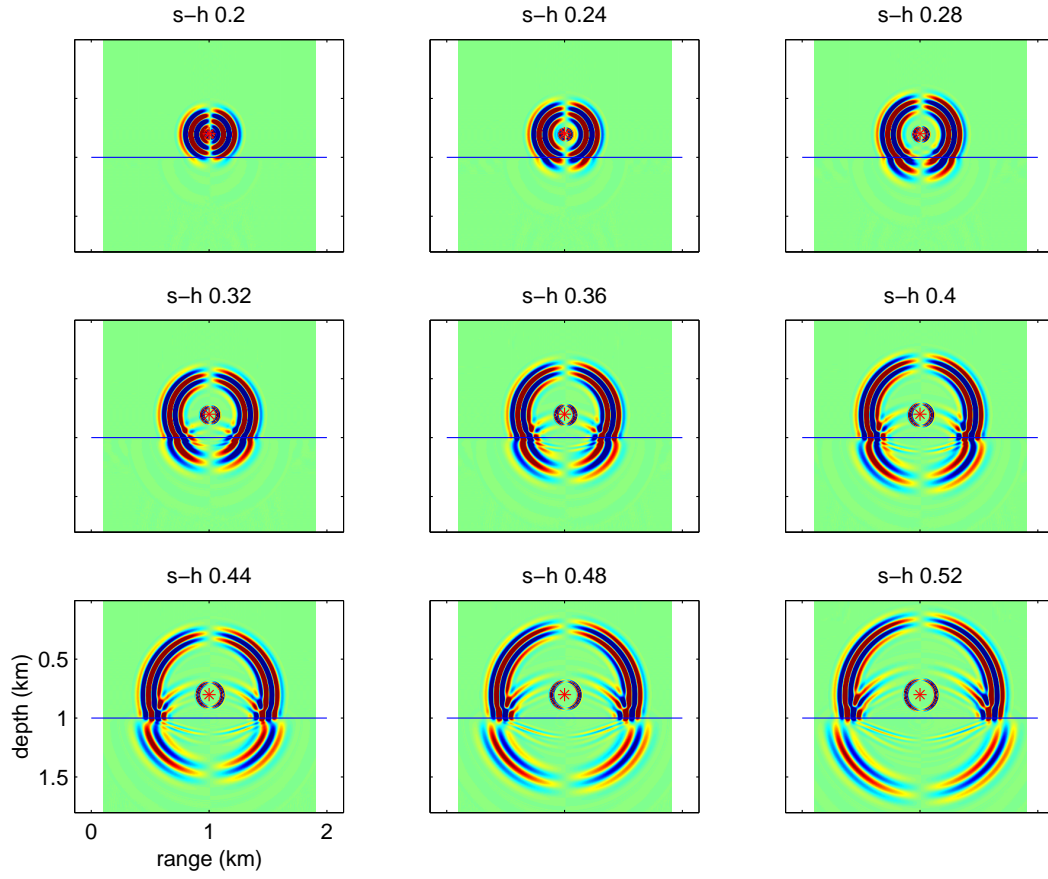


Figure 6: Snapshot of vertical solid displacements for fluid saturated limestone with gas above the interface at 1 km depth and water below, for the material parameters see ta:mat. [dutta2]

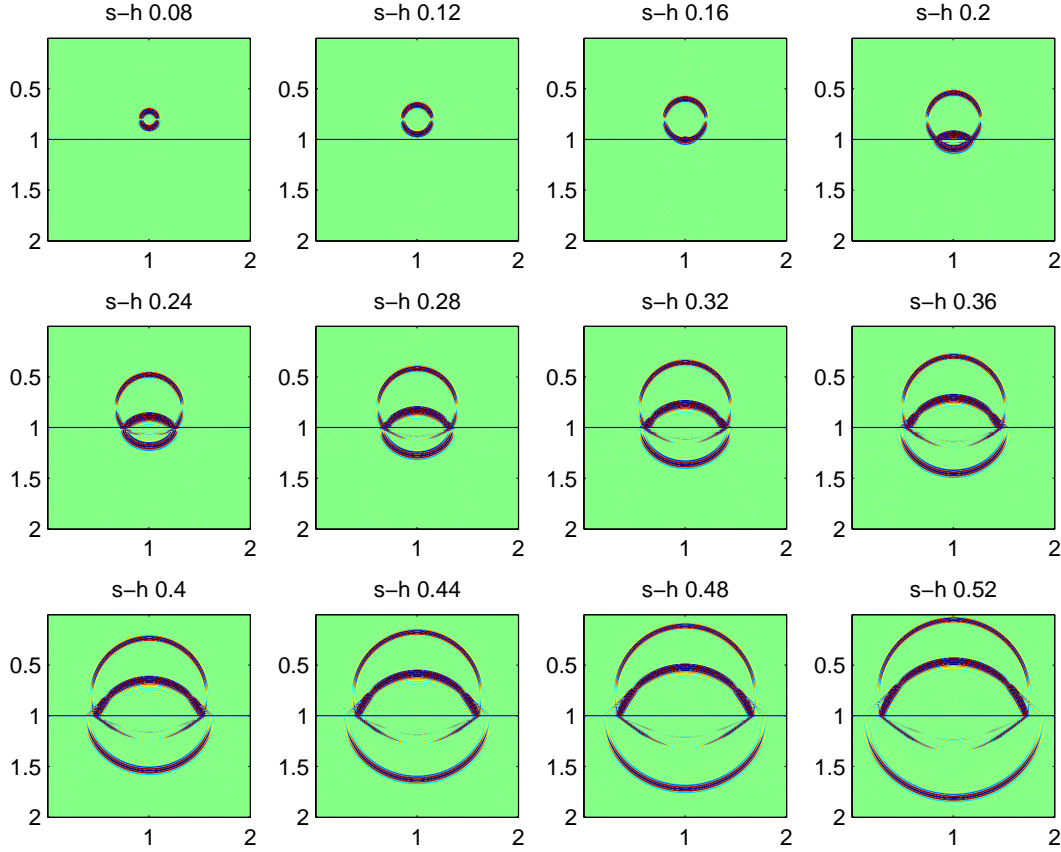


Figure 7: FD Propagation across a water/Biot interface. Top halfspace is water ($c_p = 1500$ m/s, $\rho = 1000$ kg/m³) whereas the bottom is Biot media with water saturated limestone properties. **[water]**

5.2 Poroelastic media, benchmarking

In order to benchmark the Biot FD solution, the upper halfspace in the previous example is replaced with water ($c_p = 1500$ m/s, $\rho = 1000$ kg/m³). This is done because OASES[20] does not allow sources in Biot media. The FD solution is displayed in Fig. 7.

5.3 Sloping bottom

Slowly sloping interfaces with a strong contrast is a problem for many propagation codes. For the pseudo spectral method this has been examined by several authors [Fornberg and others]. Early attempts included transformation of the grid so that all interfaces was horizontal or vertical. This appears now to be too complicated and it is instead preferred to use a denser grid at the expense of more CPU-time.

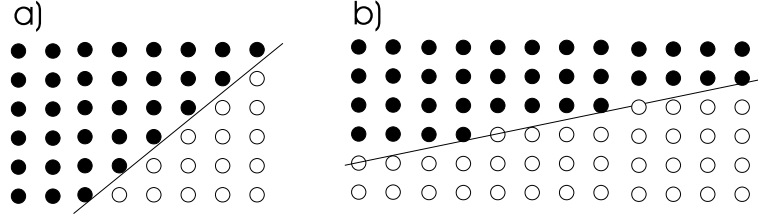
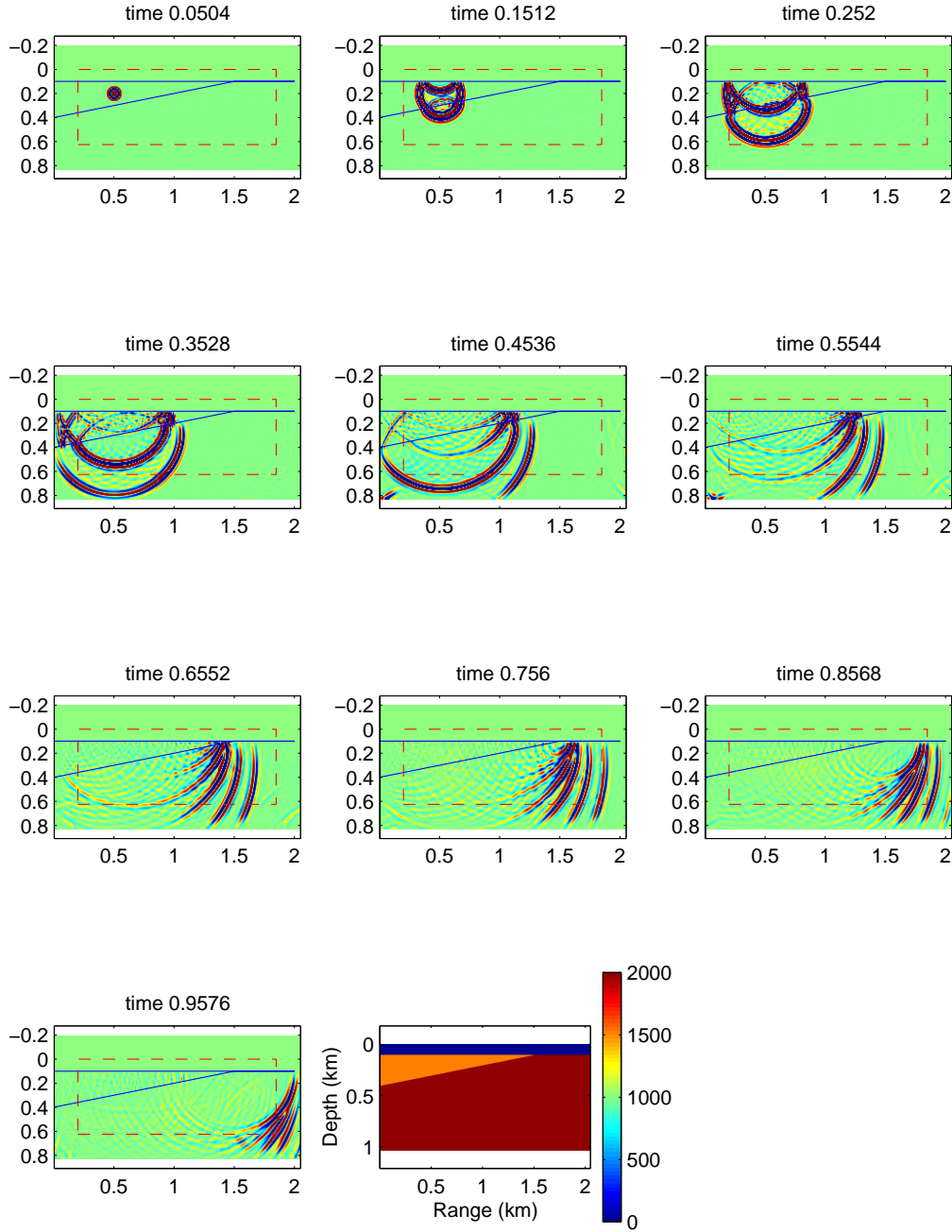


Figure 8: The change in grid properties between two media. a) A near 45° slope, b) a near horizontal slope. The interface appears less smooth in b). This indicates that in order to model an interface with low or a steep slope it is necessary to increase the grid sampling. [fdslope]

An explosion is placed at mid-water depth (100 m) 1 km from the shore. The sound speed in the water is 1500 m/s and in the bottom 2000 m/s. The seabottom has a slope of 5:1. The air/sea interface is modeled by a layer with zero sound speed. The environmental model is indicated in the lower right corner of Fig. 9. The centre frequency of the Ricker wavelet is 40 Hz. Thus the wavelength is about $\lambda = 40$ m. When modeling this case using the sampling rules in Sect. A.6 it is found that a $dx = dz = 8$ m are sufficient. Thus we use $nx=256$ and $nz=128$. The result of this modeling is seen in Fig. 9. It is clear that there are several spurious waves scattered from the seafloor. This is due to the small slope of the bottom. With a regular grid spacing of 8 m and a slope of 1:5, only every $5 \cdot 8 = 40$ m (=one wavelength) will there be an abrupt change in the seabottom, see Fig. 8. In order to avoid the scattering of the reflected waves a denser sampling is required. This problem is similar to the one encountered when modelling an ocean bottom by stair steps[22]. In Fig. 10 the vertical sampling is increased to $(dz, nz) = (3\text{m}, 400)$ while the horizontal sampling is unchanged. This corresponds to a change in bathymetry every 16 m $= 0.4 \lambda < \lambda/2$. All the spurious waves has disappeared from Fig. 10.

For the same geometry the bottom is modeled as elastic medium with $c_p=2000$ m/s and $c_s = 1000$ m/s. Due to the lower shear speed it is also necessary to decrease the grid spacing to $(dx, dz) = (8\text{m}, 1.5\text{m})$, while the grid size remains 256×400 . The lower minimum velocity combined with the denser sampling calls for a smaller time step, $dt = 0.15$ ms. The smaller time sampling causes the waves to spend more time samples (but the same amount of time) in the sponge layer and also increases the impedance contrast from non-sponge to sponge layer. This causes strong reflections from the sponge layer, Fig. 11, which early destroys the wave field.

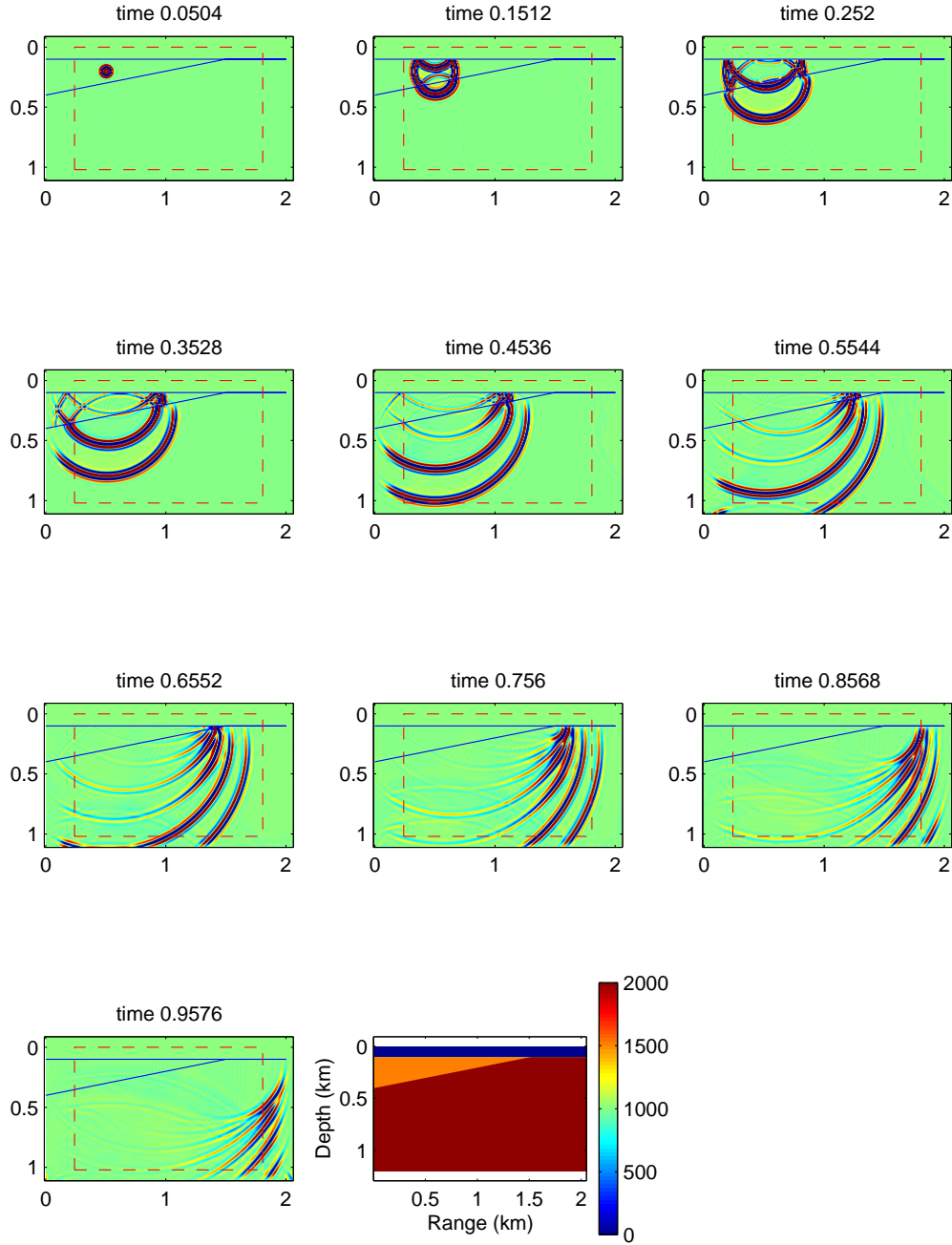
In order to correct the above, the attenuation in the sponge layer is decreased, 30 point with $\beta = 0.010$ is now used. The number of grid points is increased to 256×800 as this delays the arrival of the false reflections. The snapshots for horizontal displacements (Fig. 12) and pressure [see Eq. A10] (Fig. 13) does now appear more correct. In the pressure snapshots (Fig. 13) some weak backscattering can be seen from the top of the apex. Also, the horizontal displacements (Fig. 12) show back-scattered shear waves in the bottom, the reason for these back-scattered waves is not yet clear.



File: /cli01/gerstoft/ld/beach/acu2/ ; Date: 03-Jan-1999

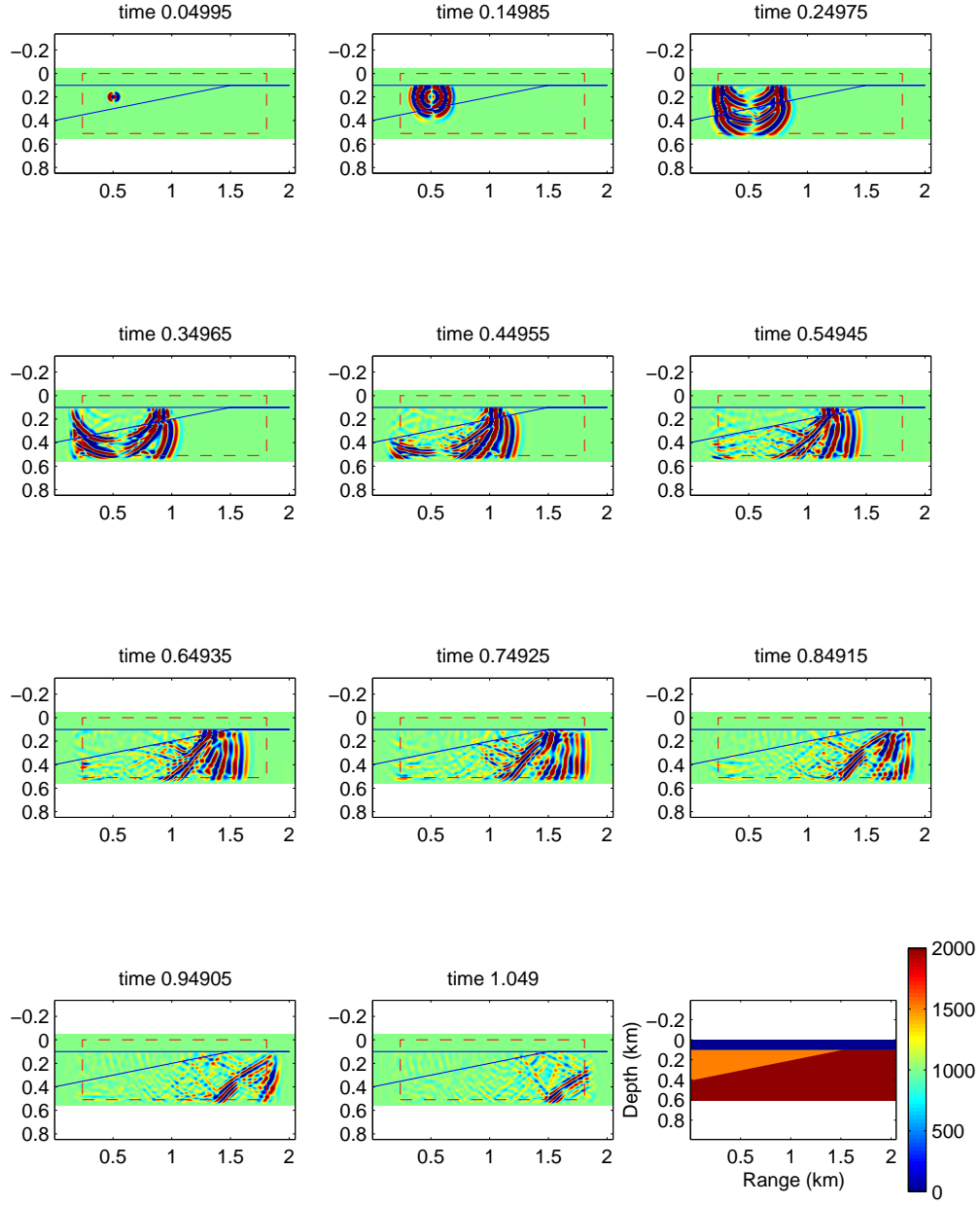
Figure 9: Pressure snapshots for acoustic sloping bottom with $c_p = 2000$ m/s. Spurious reflections from the seabottom interface is noticed. This is due to the fact that the sampling of the field and geometry is not dense enough to sample the seabottom, $(dx, dz) = (8\text{m}, 8\text{m})$ and $(nx, nz) = (256, 128)$. In the sponge layer, outside the dashed red box, the field is tapered.

[beach0]



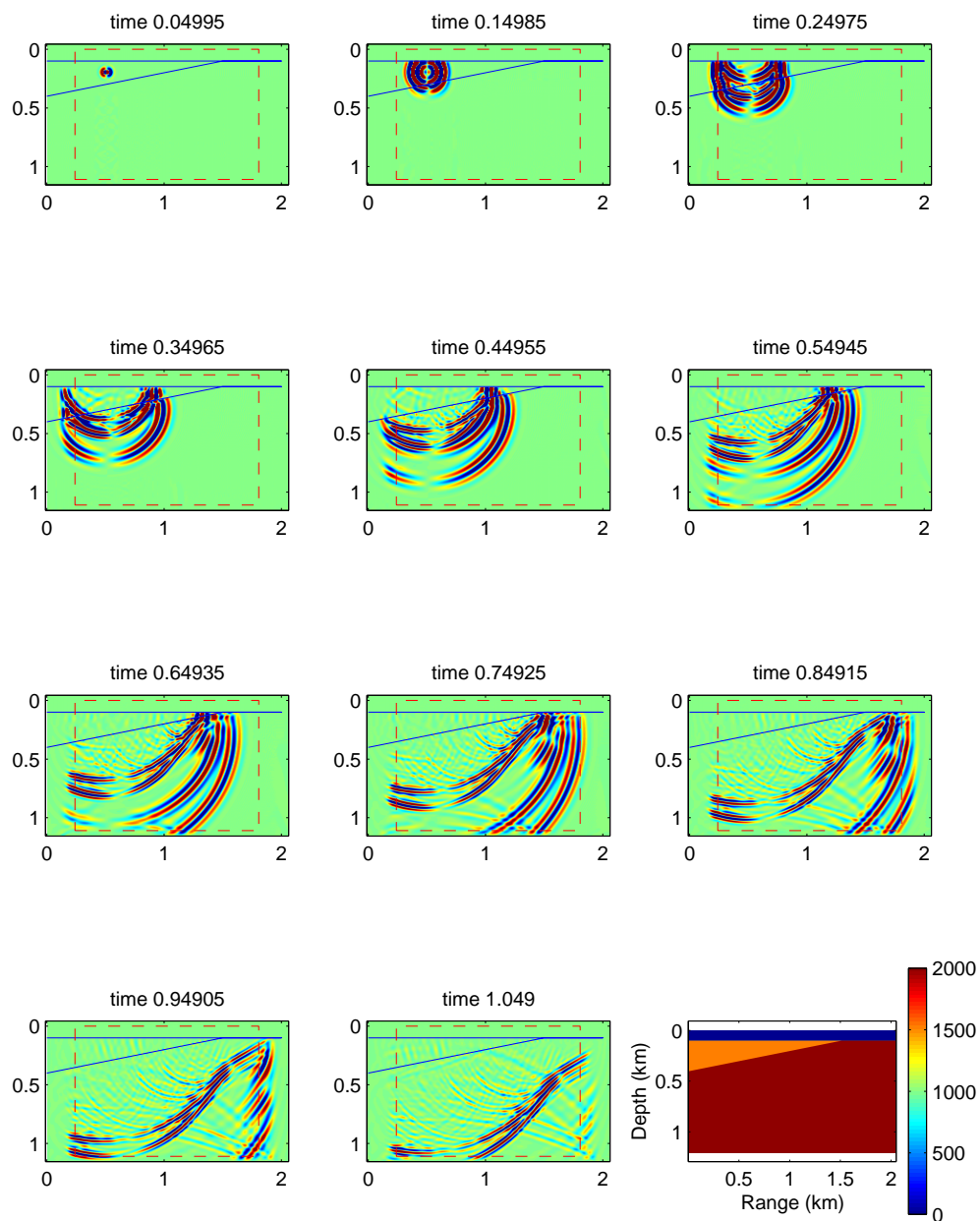
File: /cli01/gerstoft/fd/beach/test/ ; Date: 03-Jan-1999

Figure 10: Pressure snapshots for acoustic sloping bottom with $c_p=2000$ m/s. No spurious waves are observed with $(dx, dz) = (8\text{m}, 3\text{m})$ and $(nx, nz) = (256, 400)$. [beach]



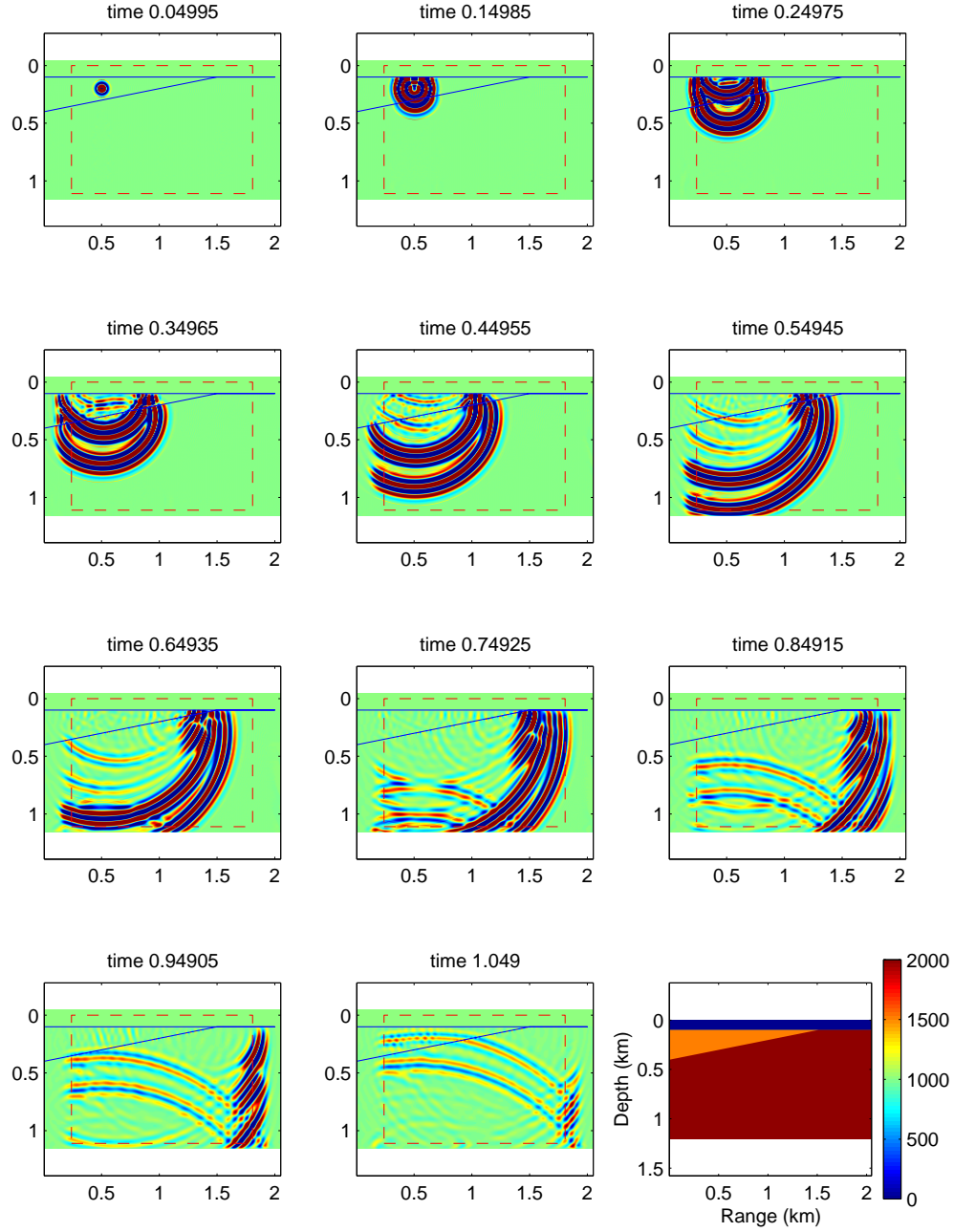
File: /clic1/gerstoftfd/beach/elas/ ; Date: 05-Jan-1999

Figure 11: Horizontal-displacements snapshots for elastic sloping bottom with $c_p=2000$ m/s and $c_s = 1000$ m/s are displayed. Reflections from the sponge layer disturb the snapshots. In the sponge layer, outside the dashed red box, the field is tapered. [**beach10**]



File: /clio1/gerstoftfd/beach/elas/ ; Date: 06-Jan-1999

Figure 12: Horizontal-displacements snapshots for acoustic sloping bottom with $c_p=2000$ m/s and $c_s = 1000$ m/s are displayed. In the sponge layer, outside the dashed red box, the field is tapered. [**beachelh**]



File: /clio1/gerstoft/td/beach/elas/ ; Date: 06-Jan-1999

Figure 13: Pressure snapshots for acoustic sloping bottom with $c_p=2000$ m/s and $c_s = 1000$ m/s are displayed. In the sponge layer, outside the dashed red box, the field is tapered. [beachelpr]

5.4 Time reverse mirror

An interesting application is to time reverse the recorded field at a set of receivers and then propagate it back into the medium. For a set of receivers around the source it is expected that this field converges at the original source. Several studies has shown that a line of receivers is sufficient to get a convergent field at the source.

5.4.1 One interface

First we investigate the field from the example in Sect. 5.1.1. Here the source was located at $(x,z) = (1200 \text{ m}, 600 \text{ m})$. At depth 660 m the range-stacked time-series are shown in Fig. 14(top) where the direct arrival is seen to arrive first close to the source range, the second arrival is the reflected arrival.

At range 500 m (700 m from the source) the depth-stacked time-series for pressure are recorded Fig. 14(middle). The transmitted wave (at 900–1600 m depth) and the direct and reflected wave (at 0–800 m depth) can easily be identified. This field is then time reversed [Fig. 14(bottom)] and used as sources for back-propagating the field. The back-propagated field are recorded at a set of receivers at depth 600 m (Fig. 15 top) and a set of receivers at range 1200 m (Fig. 15 bottom). It is seen that the field now converges close to the original source location $(x,z) = (1200, 600)$. The location is not so sharp, this is probably due to that we did not sufficiently surround the source.

5.4.2 High frequency, acoustic case

In this example we study wave propagation towards a ragged surface. The environment consists of a left medium with $c_p = 1500 \text{ m/s}$ and a right medium with $c_p = 3000 \text{ m/s}$. The density is constant. The geometry is indicated in Fig. 16. The source has a center frequency of 1 MHz and is located at $(x,z) = (2, 3) \text{ cm}$. 400×400 grid points is used with a spacing of 0.4 mm and the time step was $0.02 \mu\text{s}$. While the dimensions and frequency are unusual for seismic applications it can easily be scaled to realistic dimensions.

Snapshots of the propagation is shown in Fig. 16. In addition to all the reflections and transmissions notice the significant diffractions from the corners and strong waveguide propagation in the second slot. We record the timeseries in 15 receivers located at 14-cm range, i.e. in the second medium relative to the source, Fig. 17(top). These signals are time-reversed [Fig. 17(bottom)] and are retransmitted from the receivers at 14-cm range. Snapshots of the time-reversed field is displayed in Fig. 18. In the first set of snapshots the contribution from each individual source is quite distinct, while later it is not possible to find the origin of each wave. At around $t = 0.088 \text{ s}$ the field has converged at the original source position.

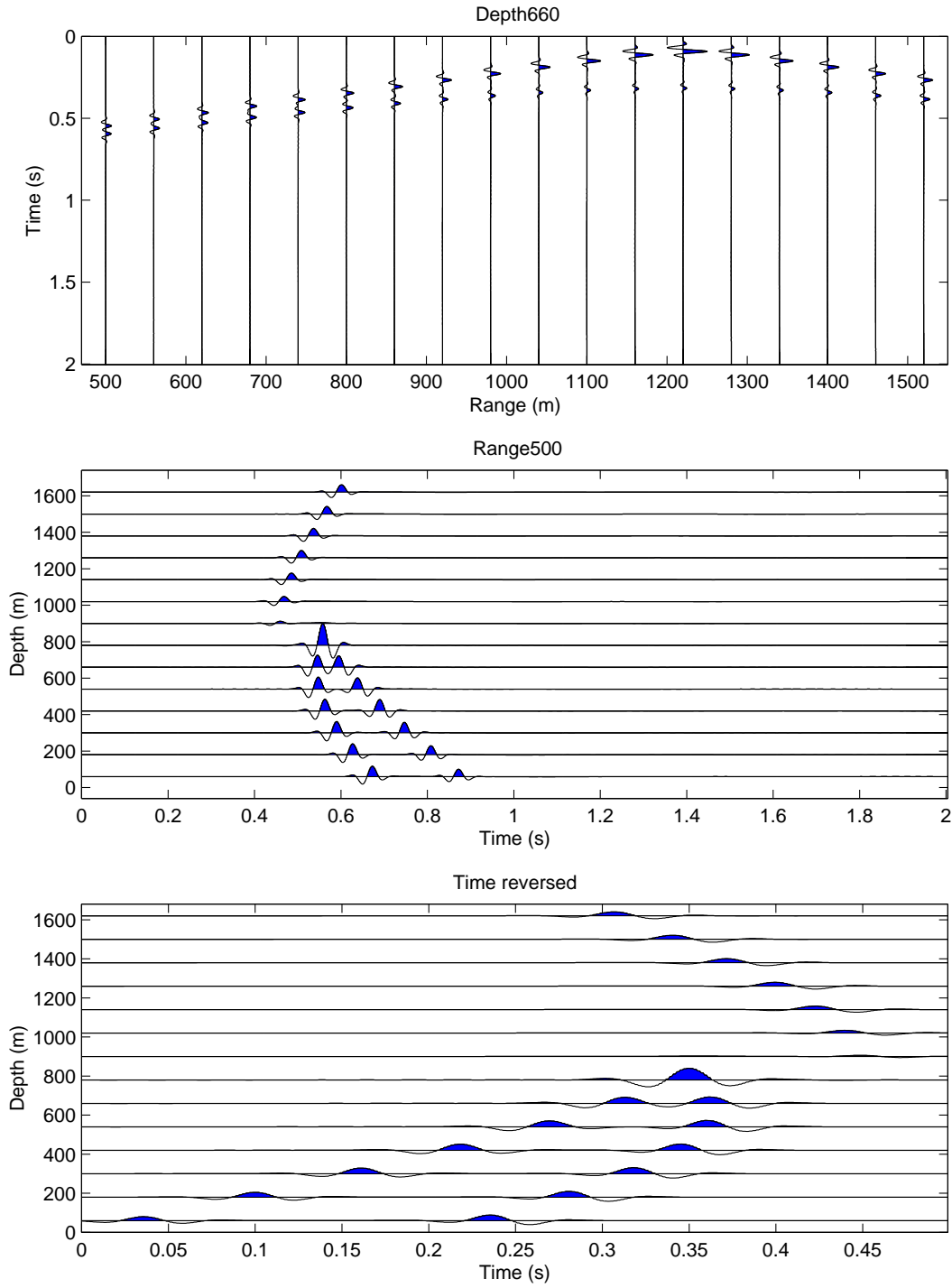


Figure 14: Stacked pressure timeseries. Top: range-stacked timeseries at a depth of 660 m, middle: depth-stacked timeseries at a range of 500 m, bottom: time-reversed depth-stacked timeseries (from 0.4–0.9 s) based on the timeseries at range 500 m. [acutimrev1]

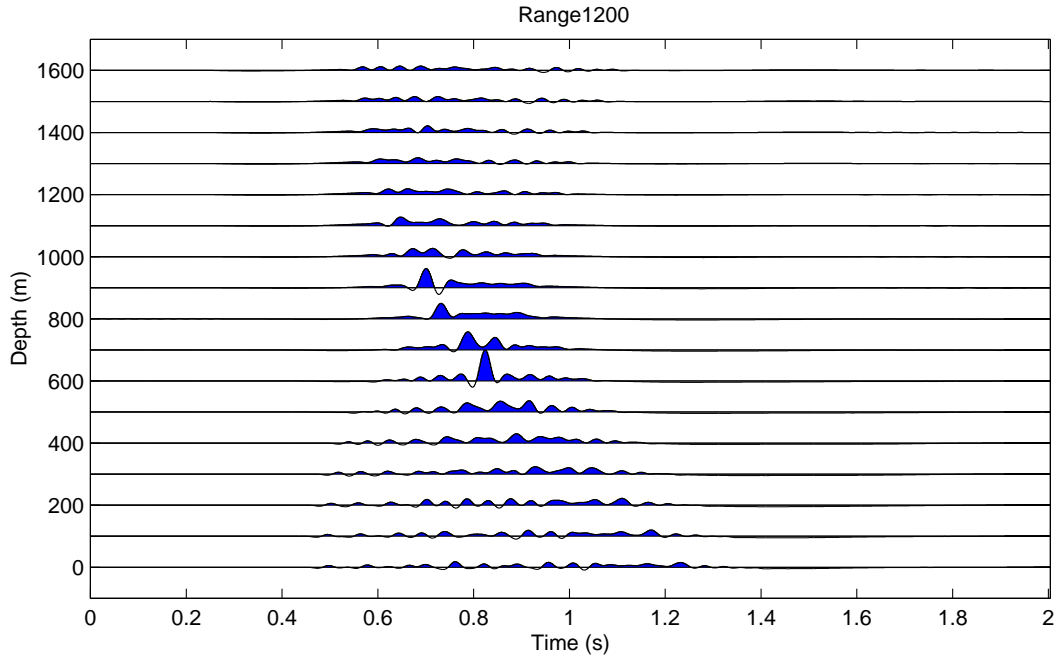
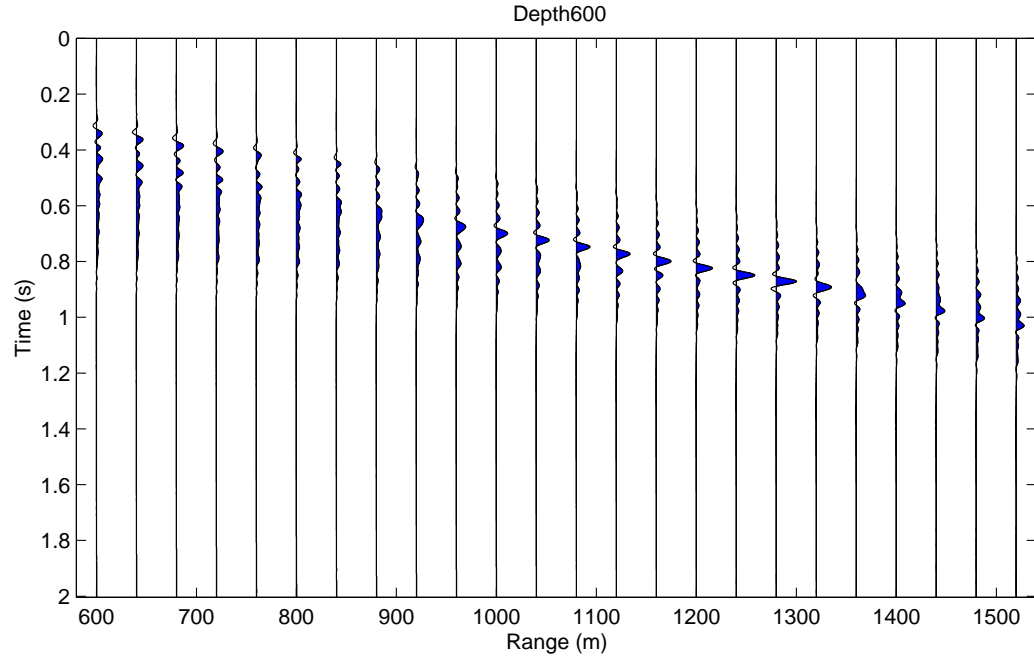


Figure 15: Using the time reversed signal in bottom plot of fig 14 as a source. The signal should now focus on the original source location $(x,z) = (1200 \text{ m}, 600 \text{ m})$. Top: range-stacked timeseries at 600-m depth, bottom: depth-stacked timeseries at 1200-m range. [**acutimrev2**]

It is noticed that a lot of energy travels in the waveguide between 2 and 4 cm depth. This is probably a main factor in the good focalization of the original source. An interesting question is if one time-reversed signal is sufficient to focus the energy at the source. By choosing the receiver at the same depth as the waveguide [(x,y)= (3,14) cm] a good excitation of the waveguide is hopefully obtained. Snapshots of the time-reversed propagation is seen in Fig. 19. The signal does converge at about $t = 0.088$ s, though there is more scatter in this plot than when using multiple of receiver/sources.

5.4.3 Elastic media, high frequency

The elastic media is interesting in a time-reversed mirror connection as it is a vector field and thus both the horizontal and vertical displacements at each receiver should be used to focus the field at the source. However, just as the receivers is not always circumventing the source in the acoustic case it might be possible to use one of the vector components when back propagating the field.

The example in the previous section is now repeated for the same geometry but using an elastic media. To the left of the solid line $c_p = 1500$ m/s, $c_s = 750$ m/s and to the right $c_p = 3000$ m/s, $c_s = 1500$ m/s. The density is constant. The center frequency is 1 MHz, 400×400 grid points are used and $dx = dy = 0.4$ mm; i.e the total dimension in x and y are 16 cm.

The snapshots for horizontal velocities are shown in Fig. 20. The wavefield is now considerable more complicated than for the acoustic case. The corresponding timeseries are shown in Fig. 21 for both the horizontal (left column) and vertical (right column) displacements. The time-reversed signal can then be back propagated. To be done!

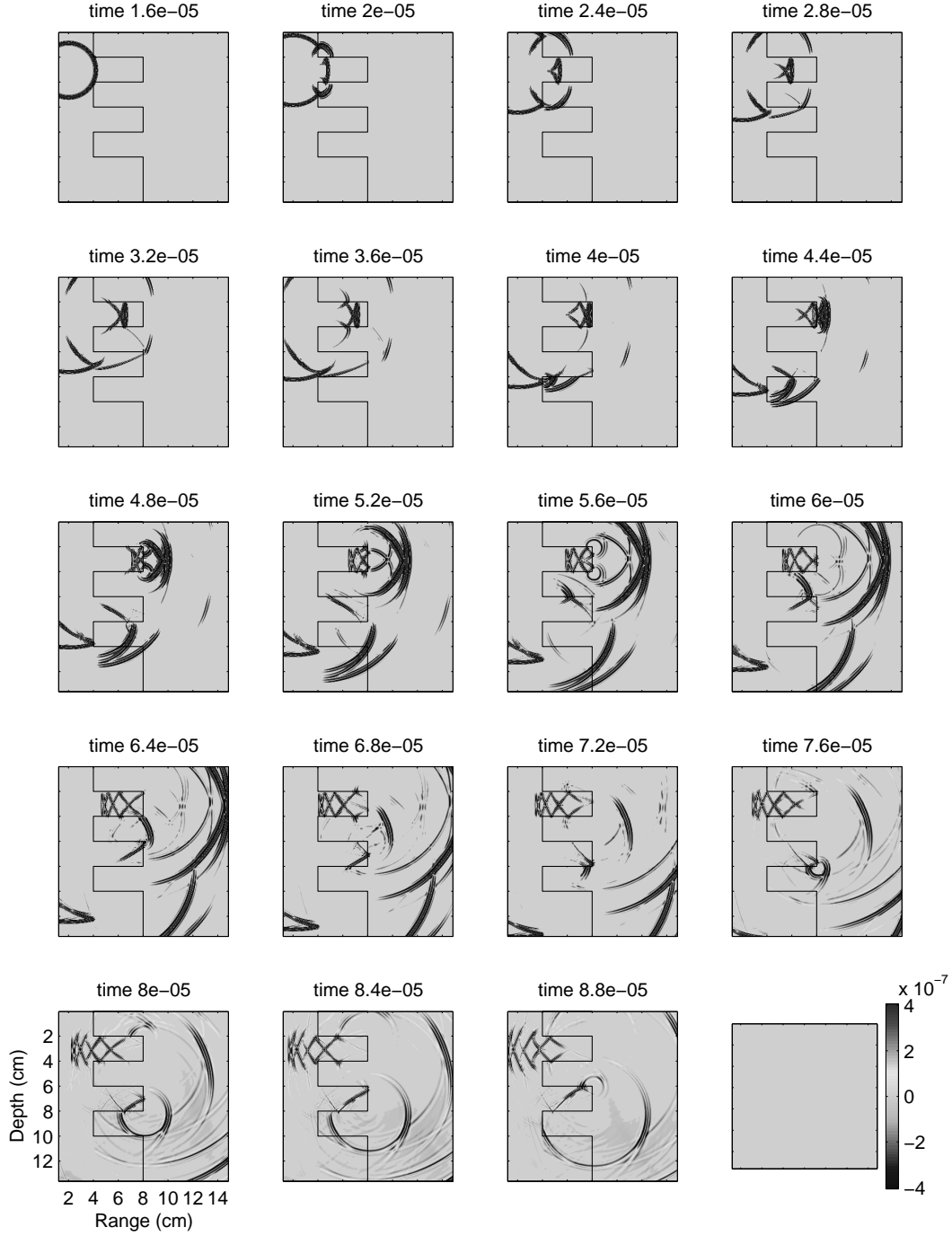


Figure 16: Snapshot of pressure for high frequency acoustics example. To the left of the solid line $c_p = 1500$ m/s and to the right $c_p = 3000$ m/s. The density is constant. The center frequency is 1 MHz, 400 grid points is used in both x and y direction $dx = dy = 0.4$ mm. $dt=0.05\mu s$ with 1000 time steps. [heechun]

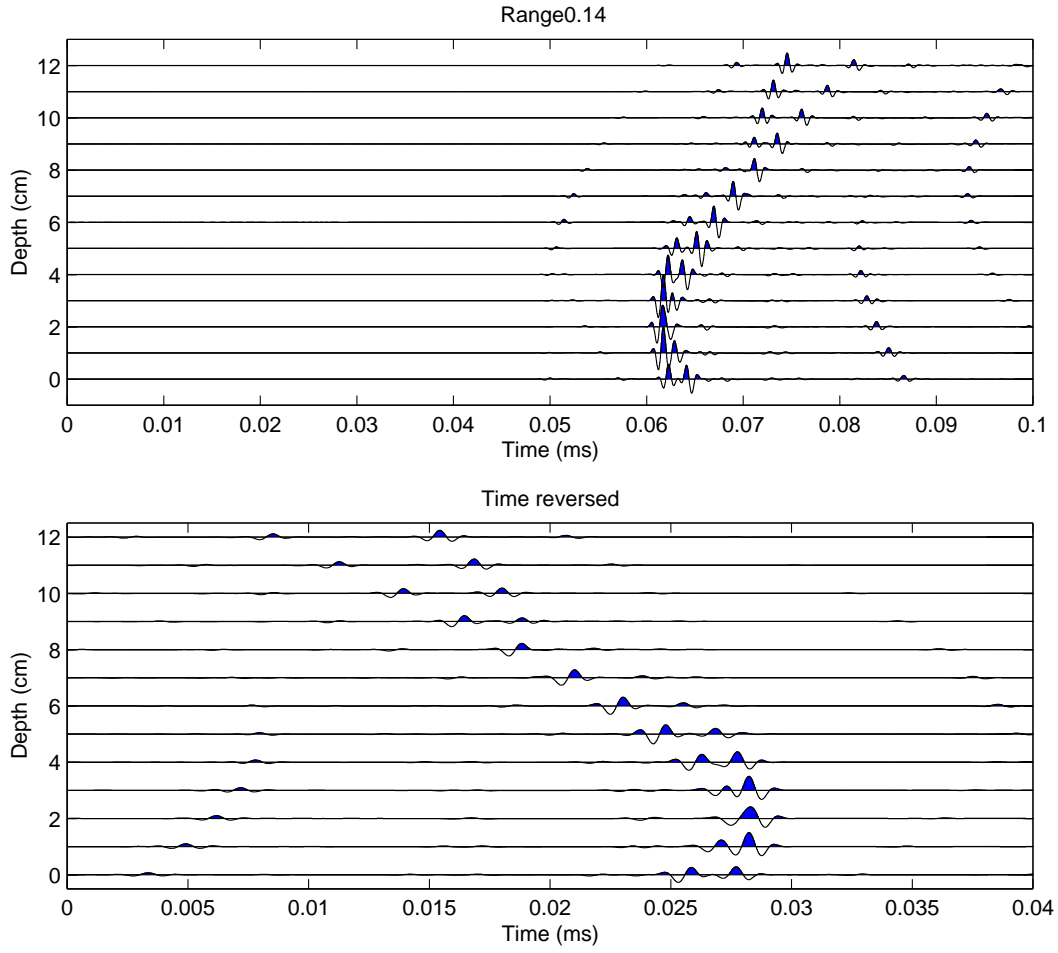


Figure 17: Depth-Stacked timeseries for the forward problem. The media are the same as in previous figure. Top: timeseries at range 14 cm, bottom: time-reversed timeseries (from 50–90 μs) [heechunseis]

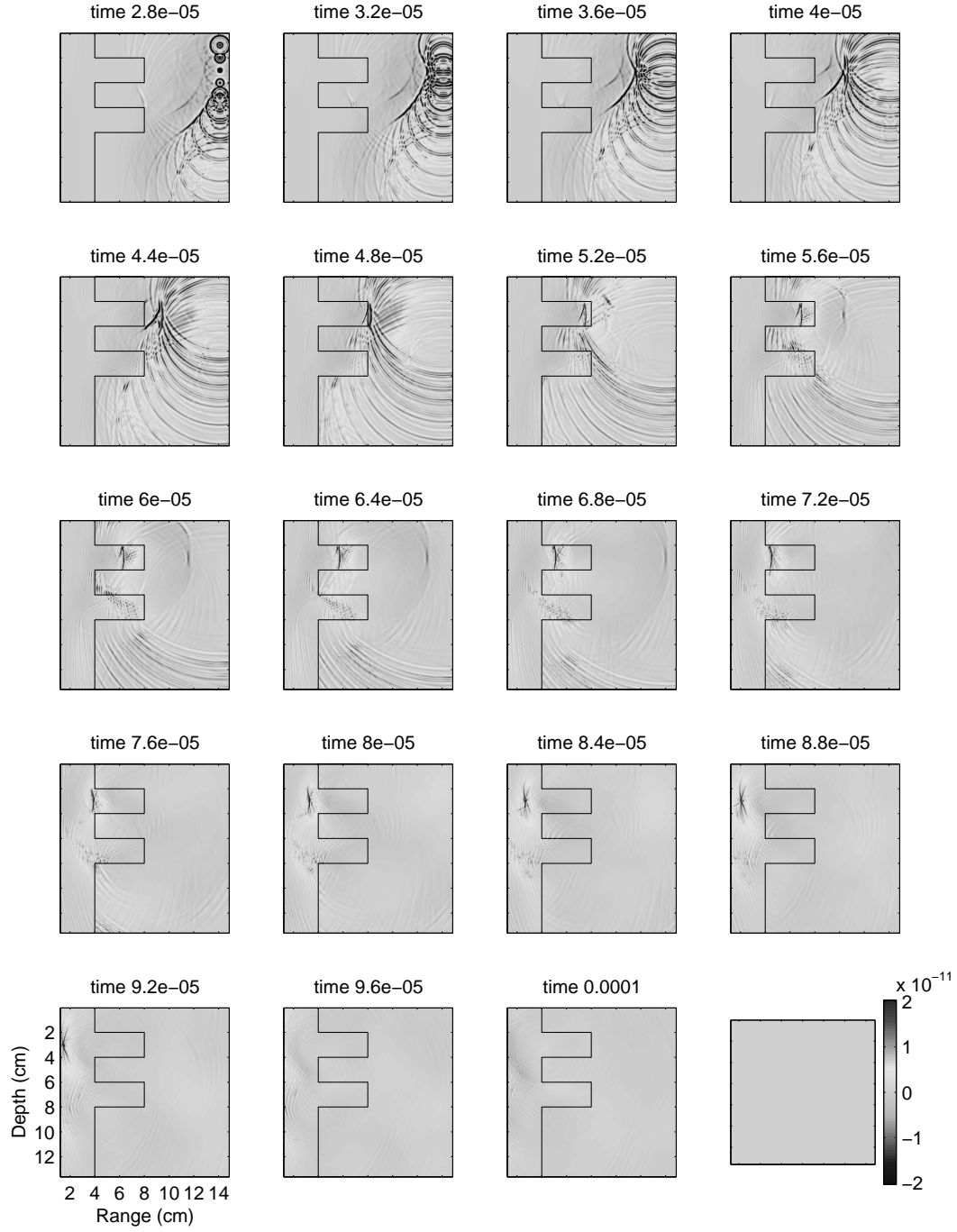


Figure 18: Time focalization for acoustic media. The signal should now focus on the original source location $(x,z) = (2,3)$ cm, and this happens at about $t=0.088$ ms. [heechuntimrev]

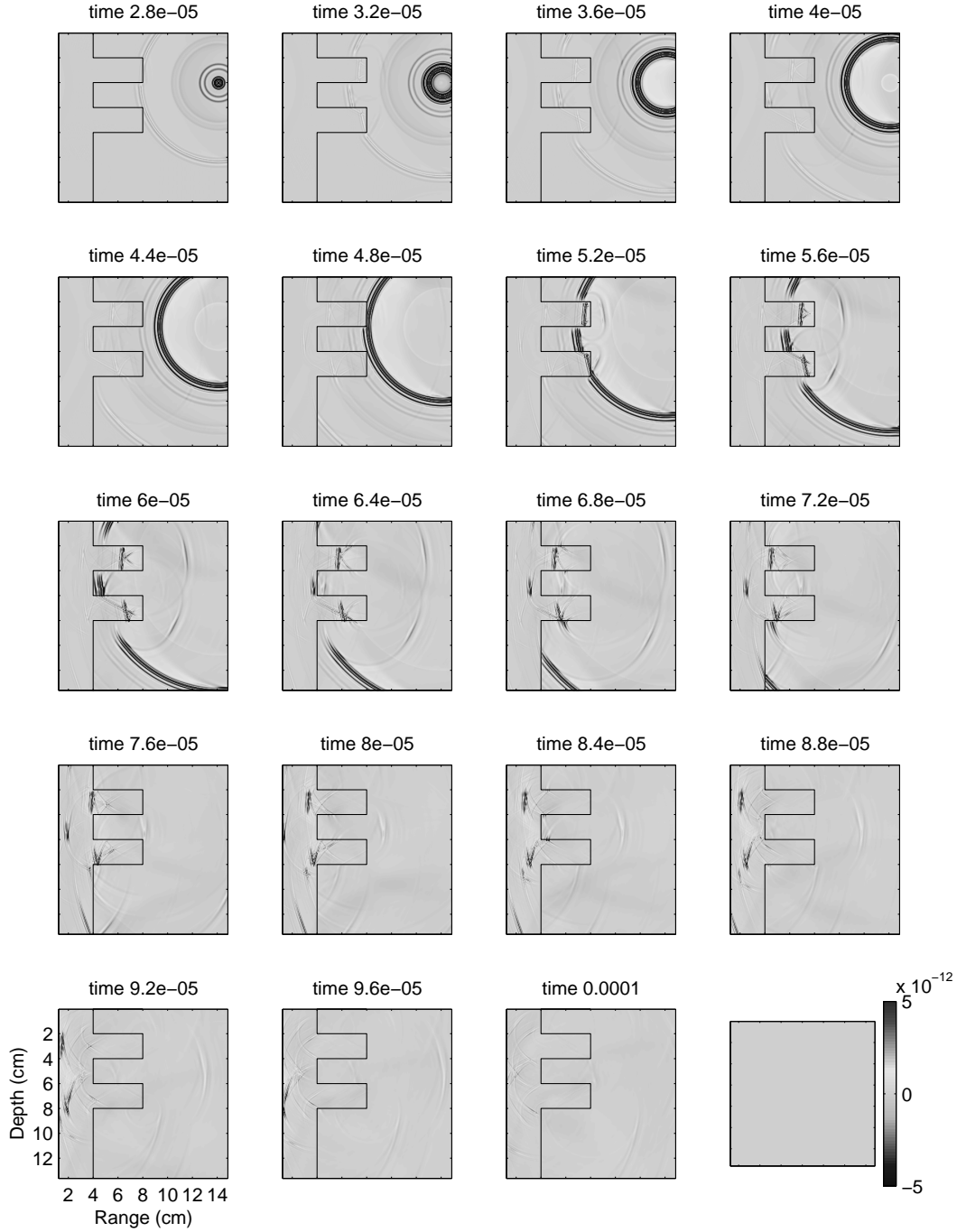


Figure 19: Time focalization for acoustic media using one source. The signal should now focus on the original source location $(x,z) = (2,3)$ cm, and this happens at about $t=0.088$ ms. [heechuntimrev1]

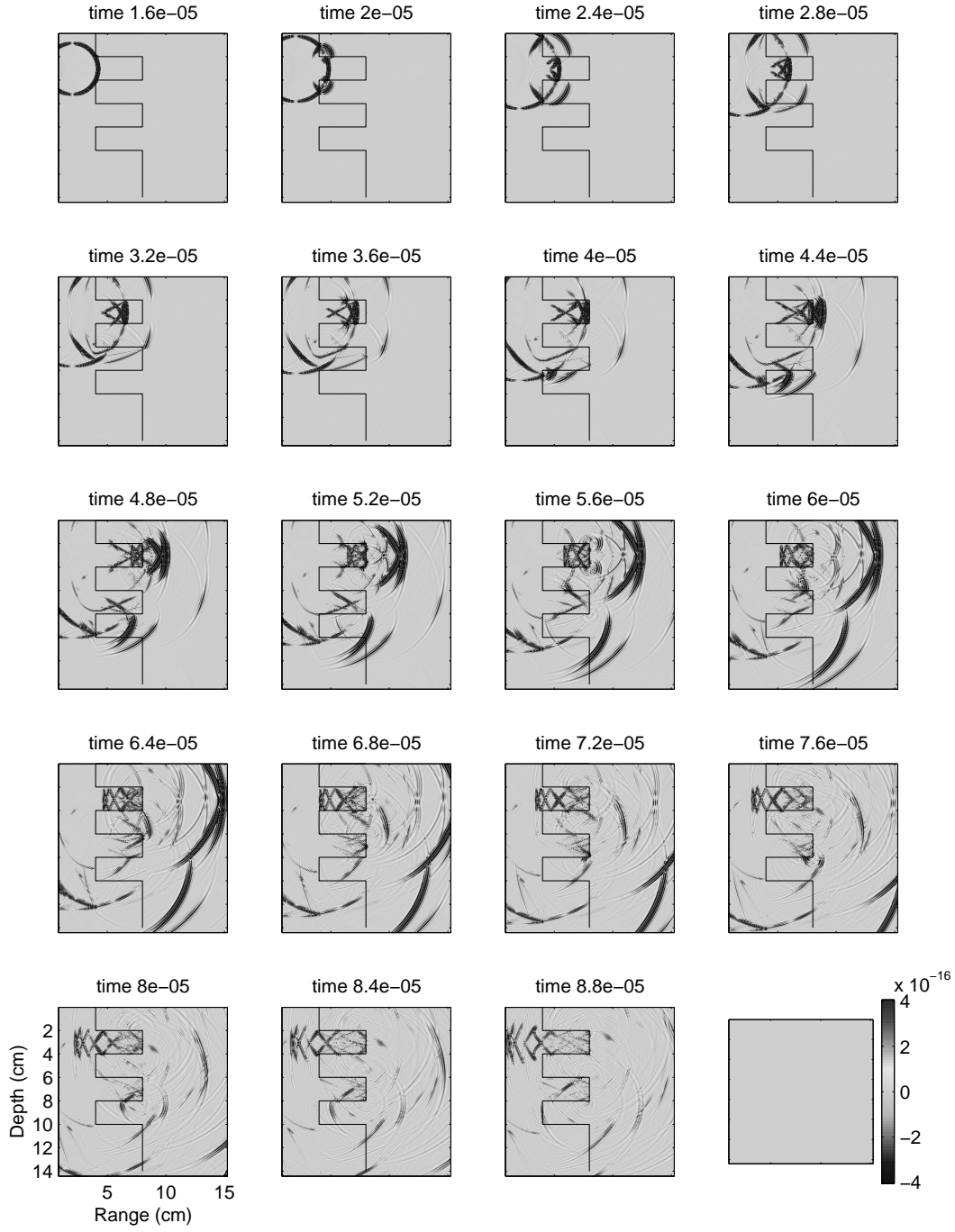


Figure 20: Snapshots of horizontal velocities for the elastic example. `[hcElasSnap]`

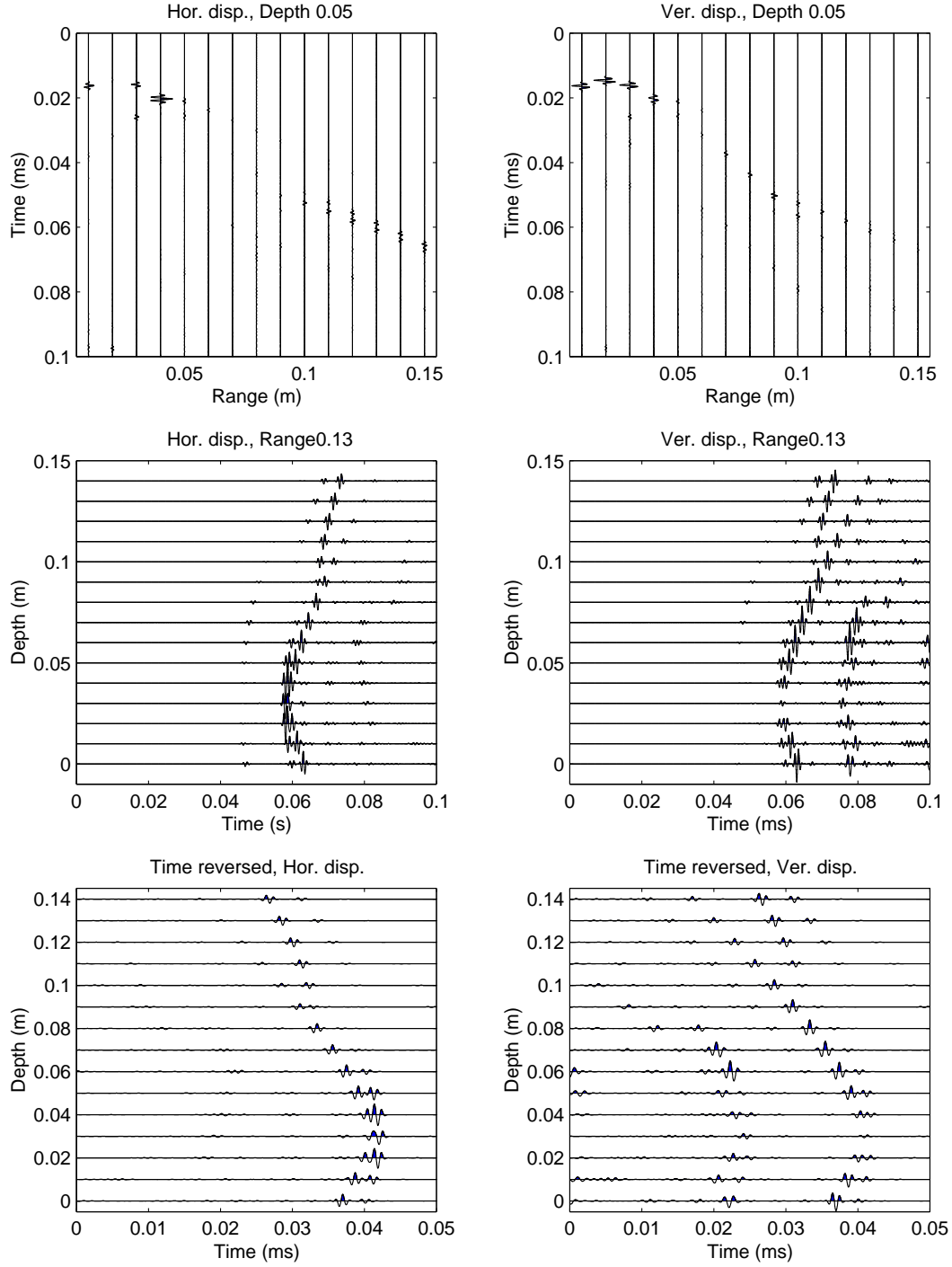


Figure 21: Timeseries for horizontal (left column) and vertical (right column) displacements. Top row: range-stacked timeseries at depth 5 cm, middle row: depth-stacked timeseries at range 13 cm, bottom row: time-reversed depth-stacked timeseries (from 0.05–0.1 ms) [hcElasSeis]

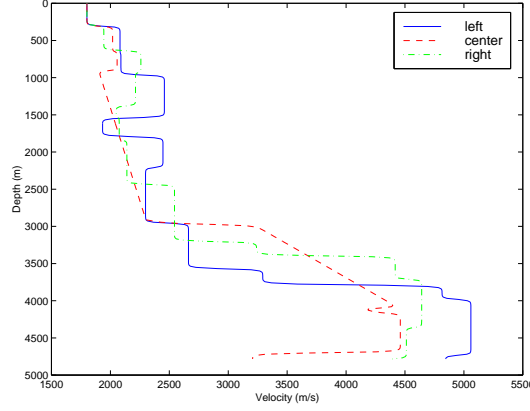


Figure 22: Three P-velocity profiles from the left (full), center(dashed) and right (dash-dotted) of the dome at Tommeliten. [tomelvel]

5.5 Tommeliten

A small study of modeling the reflections from a marine environment as Tommeliten [23] was performed. Tommeliten is an oil field in the North Sea and here the velocity field from this environment is used. Three P-velocity profiles was used, see Fig. 22. We here assume that the left, center and right profile are at distance 0, 3 and 6 km, respectively. We use a source placed in the top water layer at depth 60 m and range 3 km and with a center frequency of 20 Hz. The grid spacing was 20 m and base on linear interpolation of the profiles the P-wave velocity field in Fig. 23 was obtained. We have here neglected the sea surface.

The result of the FD modeling is shown in Fig. 24. The color scale is the same in all frames. The high gain used is evident in the first set of frames as the waves does not appear well defined. The major reflection seen at about $t = 1.5$ s is the reflection from the Top Balder layer (the reflector at 3000 m depth). The low frequency and amplitude (blue) waves are reflections from the sponge layer. While they disturb the appearance of the snapshots, they have little influence on the seismograms, as seen in Fig. 25. The small reflection at $t = 3$ s in Fig. 25 is from the Top Balder layer.

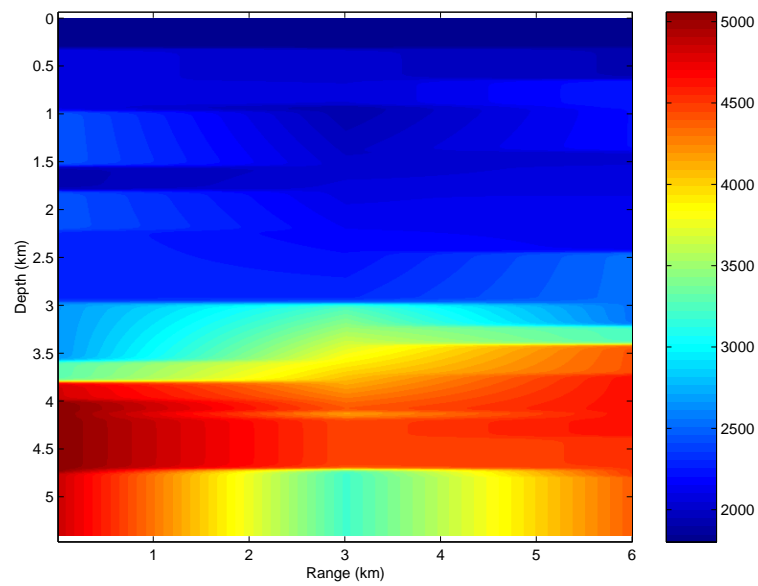


Figure 23: A range dependent P-velocity structure. Based on three velocity profiles from the Tommeliten. [**acuvel**]

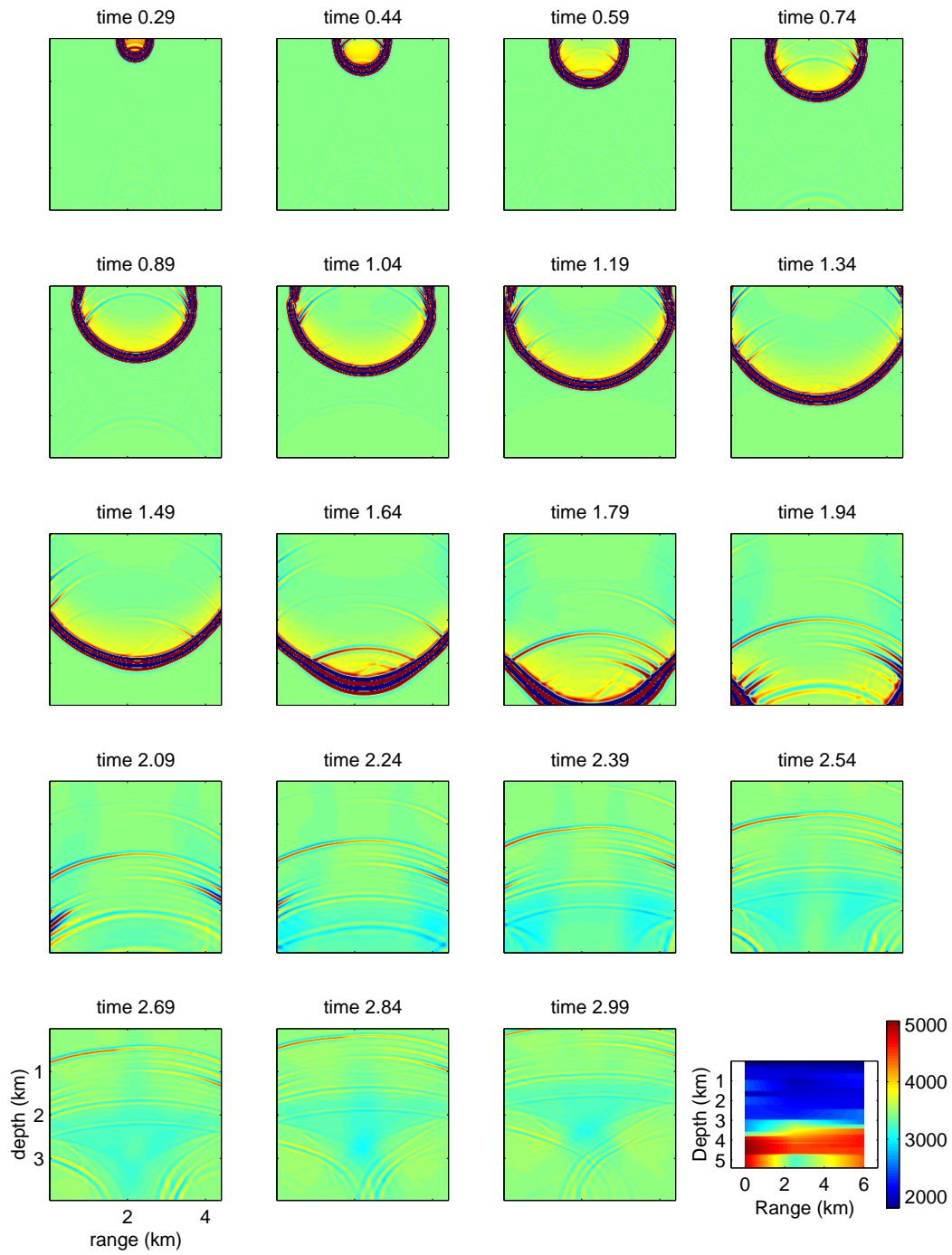


Figure 24: Snapshot of pressure, each panel shows the time evolution of the field. [tomoliten]

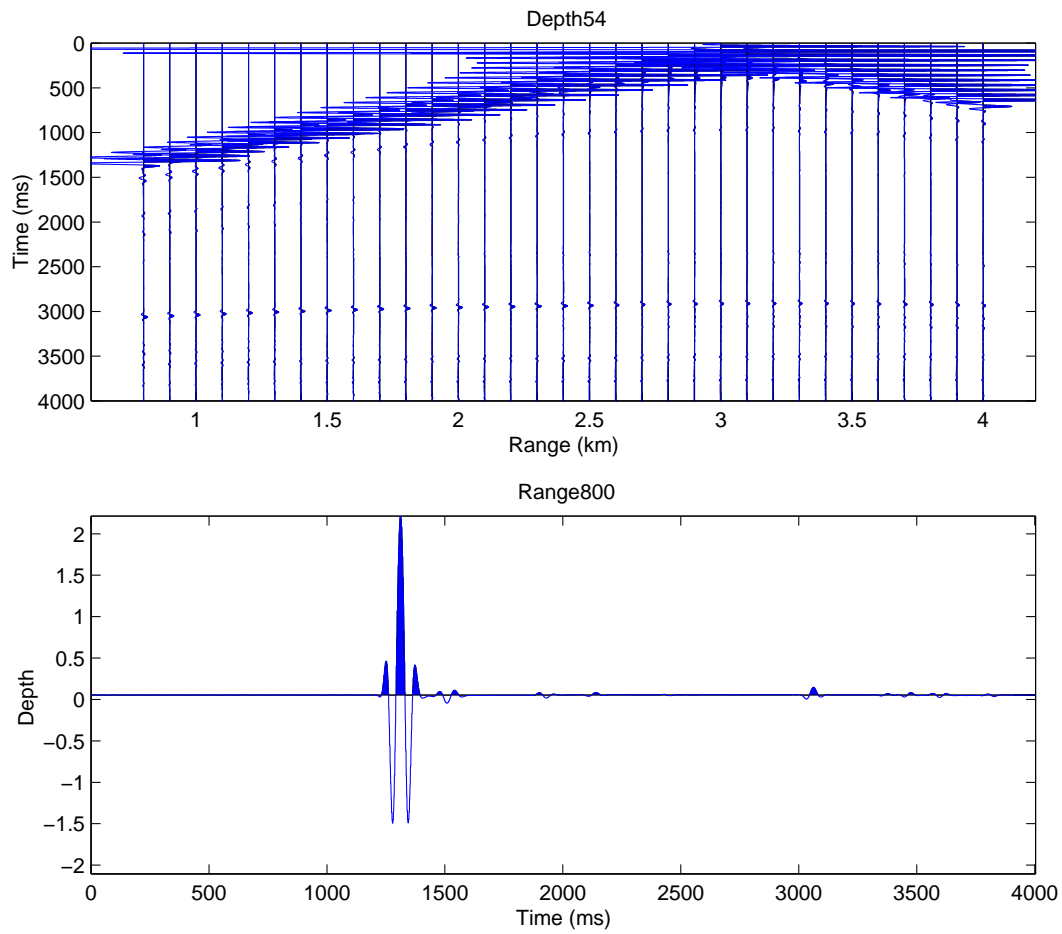


Figure 25: Seismograms from Tommeliten. a) Range stacked timeseries of pressure at a depth of 54 m (a gain of 100 is used). b) Single time series at a range of 800 m. [tomwiggle]

A APPENDIX A: Background

A.1 Acoustic media

$$\frac{1}{\rho c^2} \frac{\partial^2 p}{\partial t^2} = \frac{\partial}{\partial x} \left(\frac{1}{\rho} \frac{\partial p}{\partial x} \right) + \frac{\partial}{\partial z} \left(\frac{1}{\rho} \frac{\partial p}{\partial z} \right) \quad (\text{A1})$$

A.2 Elastic media

$$\rho \frac{\partial^2 u_x}{\partial t^2} = \frac{\partial \sigma_{xx}}{\partial x} + \frac{\partial \sigma_{xz}}{\partial z} \quad (\text{A2})$$

$$\rho \frac{\partial^2 u_z}{\partial t^2} = \frac{\partial \sigma_{xz}}{\partial x} + \frac{\partial \sigma_{zz}}{\partial z} \quad (\text{A3})$$

$$\sigma_{xx} = \lambda(e_{xx} + e_{zz}) + 2\mu e_{xx} = (\lambda + 2\mu)e_{xx} + \lambda e_{zz} \quad (\text{A4})$$

$$\sigma_{zz} = \lambda(e_{xx} + e_{zz}) + 2\mu e_{zz} = (\lambda + 2\mu)e_{zz} + \lambda e_{xx} \quad (\text{A5})$$

$$\sigma_{xz} = 2\mu e_{xz} \quad (\text{A6})$$

The strains are

$$e_{xx} = \frac{\partial u_x}{\partial x} \quad (\text{A7})$$

$$e_{zz} = \frac{\partial u_z}{\partial z} \quad (\text{A8})$$

$$e_{xz} = \frac{1}{2} \left(\frac{\partial u_x}{\partial z} + \frac{\partial u_z}{\partial x} \right) \quad (\text{A9})$$

The pressure is then given by

$$p = -\frac{1}{2}(\sigma_{xx} + \sigma_{zz}) = -(2\mu + \lambda) \left(\frac{\partial u_x}{\partial x} + \frac{\partial u_z}{\partial z} \right) \quad (\text{A10})$$

The shear effects can be shown by plotting the shear stress σ_{xz} .

A.3 Poroelastic media

Here we are studying wave propagation in a *fluid saturated* porous media. The solid frame of the porous media is modeled as an elastic media. The analysis is based on Biot's model.

A.3.1 Material parameters

An *open system* is one where the fluid can flow out when the material is pushed; whereas in a *closed system* the fluid it cannot. A *dry material* is one without fluid and a *saturated material* is one the pores are filled with fluid. For our purpose an open system correspond to a dry material and an closed system to a saturated material.

Several authors has investigated the properties of porous media [18, 16, 19, 15, 17] and several material parameters are introduced. These are not all independent. Some of the common used material parameters are:

λ is the Lamé constant of the saturated material (closed system)

λ_0 is the Lamé constant of the open system $\lambda_0 = \lambda - \alpha^2 M$

μ is the shear modulus of the (dry or saturated) porous material

$M = [\phi/K_f + (\alpha - \phi)/K_s]^{-1} = [\phi/K_f + (1 - \phi - K_b/K_s)/K_s]^{-1}$. M is the pressure to be exerted on the fluid to increase the fluid content by one at isovolumetric strain ($e = 0$)

$\alpha = 1 - K_b/K_s$

$C = \alpha M$

K_b is the bulk modulus of the dry (open) frame $K_b = \lambda_0 + \frac{2}{3}\mu$

K_s is the bulk modulus of the grains alone

K_{sat} is the bulk modulus of the saturated material $K_{sat} = \lambda + \frac{2}{3}\mu$

K_f is the bulk modulus of the pore fluid

$\lambda = M^{-1}C^2 + K_b - \frac{2}{3}\mu = \alpha^2 M + \lambda_0$

ρ_f pore fluid density

ρ_s solid grain density

$\rho = \phi\rho_f + (1 - \phi)\rho_s$ is the total density

ϕ porosity of the solid.

$m = a\rho_f/\phi$ is the equivalent mass for the fluid

a is the turtosity of the matrix. It is also called the structure factor or virtual mass demoted be c_m

κ permeability. It is used in the viscosity term. It is similar to the ones used in Darcy's law.

η viscosity of the fluid.

A good set of parameters for describing a Biot material are:

Fluid: $\rho_f, K_f, \kappa, \eta$.

Solid frame: $\mu, \lambda_0, \rho, K_b, K_s$.

Fluid/solid interaction: ϕ, a .

A.3.2 Zero frequency limit of P and S wave

In a Biot media three types of body wave exist: a fast P-wave (P-I), a slow P-wave (P-II) and a S-wave. The general expression for the P-I, P-II and S waves can be found in e.g. [21, 14] and this approach is also implemented in matlab programs.

In the zero frequency limit the P1 and S wave velocities are given by

$$c_p = \sqrt{(\lambda + 2\mu)/\rho} \quad (\text{A11})$$

$$c_s = \sqrt{\mu/\rho} \quad (\text{A12})$$

A.3.3 The equations

The constitutive equations are,

$$\sigma_{xx} = (\lambda + 2\mu)e_{xx} + \lambda e_{yy} + \alpha M\xi \quad (\text{A13})$$

$$\sigma_{zz} = (\lambda + 2\mu)e_{zz} + \lambda e_{xx} + \alpha M\xi \quad (\text{A14})$$

$$\sigma_{xz} = 2\mu e_{xz} \quad (\text{A15})$$

$$p = -M[\alpha e + \xi] \quad (\text{A16})$$

where

$$e = e_{xx} + e_{zz} = \nabla \cdot \mathbf{u} = \frac{\partial u_x}{\partial x} + \frac{\partial u_z}{\partial z} \quad (\text{A17})$$

$$\xi = \nabla \cdot \mathbf{w} = \left(\frac{\partial w_x}{\partial x} + \frac{\partial w_z}{\partial z} \right) \quad (\text{A18})$$

$$\mathbf{w} = \phi(\mathbf{U} - \mathbf{u}) \quad (\text{A19})$$

Where \mathbf{u} , \mathbf{U} , and \mathbf{w} are the displacements of the solid, displacements of the fluid and the differential fluid displacement, respectively. In order to interpret the physical parameters, it is useful to reorder the constitutive equations

$$\begin{aligned} \sigma_{xx} &= (\lambda_0 + 2\mu)e_{xx} + \lambda e_{zz} + \alpha p \\ \sigma_{zz} &= (\lambda_0 + 2\mu)e_{zz} + \lambda e_{xx} + \alpha p \\ \sigma_{xz} &= 2\mu e_{xz} \\ \xi &= -\frac{1}{M}p - \alpha e. \end{aligned} \quad (\text{A20})$$

The equations of motion are:

$$\frac{\partial^2(\rho u_x + \rho_f w_x)}{\partial t^2} = \frac{\partial \sigma_{xx}}{\partial x} + \frac{\partial \sigma_{xz}}{\partial z}$$

$$\begin{aligned} \frac{\partial^2(\rho u_z + \rho_f w_z)}{\partial t^2} &= \frac{\partial \sigma_{xz}}{\partial x} + \frac{\partial \sigma_{zz}}{\partial z} \\ \frac{\partial^2(\rho_f u_x + m w_x)}{\partial t^2} + \frac{\eta}{\kappa} \frac{\partial w_x}{\partial t} &= \frac{\partial p}{\partial x} \end{aligned} \quad (\text{A21})$$

$$\frac{\partial^2(\rho_f u_z + m w_z)}{\partial t^2} + \frac{\eta}{\kappa} \frac{\partial w_z}{\partial t} = \frac{\partial p}{\partial z} \quad (\text{A22})$$

At higher frequencies the viscous term will give more resistance to the motion. Thus in frequency domain formulations a frequency dependent dynamic correction term is multiplied to the viscoelastic term. As we are working in the time domain this correction term is not easily applied and is neglected here.

From the equations of motion we obtain:

$$\begin{aligned} (m\rho - \rho_f^2) \frac{\partial^2 u_x}{\partial t^2} &= +m \frac{\partial \sigma_{xx}}{\partial x} + m \frac{\partial \sigma_{xz}}{\partial z} - \rho_f \frac{\partial p}{\partial x} + \rho_f \frac{\eta}{\kappa} \frac{\partial w_x}{\partial t} \\ (m\rho - \rho_f^2) \frac{\partial^2 u_z}{\partial t^2} &= +m \frac{\partial \sigma_{zz}}{\partial z} + m \frac{\partial \sigma_{xz}}{\partial x} - \rho_f \frac{\partial p}{\partial z} + \rho_f \frac{\eta}{\kappa} \frac{\partial w_z}{\partial t} \\ (m\rho - \rho_f^2) \frac{\partial^2 w_x}{\partial t^2} &= -\rho_f \frac{\partial \sigma_{xx}}{\partial x} - \rho_f \frac{\partial \sigma_{xz}}{\partial z} + \rho \frac{\partial p}{\partial x} - \rho \frac{\eta}{\kappa} \frac{\partial w_x}{\partial t} \\ (m\rho - \rho_f^2) \frac{\partial^2 w_z}{\partial t^2} &= -\rho_f \frac{\partial \sigma_{zz}}{\partial z} - \rho_f \frac{\partial \sigma_{xz}}{\partial x} + \rho \frac{\partial p}{\partial z} - \rho \frac{\eta}{\kappa} \frac{\partial w_z}{\partial t} \end{aligned} \quad (\text{A23})$$

It has been found that In a PE-formulation only 3 equations and variables are necessary to describe the medium[14]. Physically that seems reasonable as usually two equations are needed for elastic media and one equation for the fluid media.

A.3.4 Fluid media

From a Biot media a fluid media can be obtained by having no frame, $\phi = 1$, and $\mu = 0$, $\alpha = 1$, $K_b = 0$, $a = 1$, $\rho = \rho_f = m$. This works for Eq. (A22), but for Eq. (A23) the left hand side of the equations becomes singular $[(m\rho - \rho_f^2) = 0]$, as the equations in Eq. (A22) becomes singular. Practically, In order to compute the response for a composite fluid/Biot media we approximate $\rho = 1.01\rho_f$ in the fluid media [alternatively we could have worked directly with Eq. (A22)].

A.3.5 Elastic media

From a Biot media an elastic media can be obtained by having no frame, $\phi = 0$, and $\rho_f = 0$, $\alpha = 0$.

A.4 Fourier spectral method

Pseudo spectral methods evaluate the spatial derivatives in the wavenumber domain. Consider the evaluation of $\frac{\partial U(x)}{\partial x}$ on a regular grid with N grid points and spacing h

$$\frac{\partial U(x)}{\partial x} = \mathcal{F}^{-1} [ik_x \mathcal{F}\{U(x)\}] \quad (\text{A24})$$

where $k_x = 2\pi j/h$, $j = 1, \dots, N$ is the spatial wave numbers, i is the imaginary unit and \mathcal{F} is the Fourier transform.

On a staggered grid the first derivative will be based halfway between the $U(x)$ points.

$$\frac{\partial U(x)}{\partial x} = \mathcal{F}^{-1} [ik_x e^{-ik_x h/2} \mathcal{F}\{U(x)\}] , \quad (\text{A25})$$

where the factor $e^{-ik_x h/2}$ is used to translate the $\frac{\partial U(x)}{\partial x}$ so that they are calculated on the halfway grid. When differentiating variables on the second (halfway) grid, the grid will be translated back to the original grid; the $-$ in the complex exponential in the above formula should be replaced with a $+$.

Pseudo spectral methods obtain the highest theoretically possible accuracy for a spatial differentiation. Due to the higher precision it is possible to have a less dense grid, 2 to 3 samples per wavelength is sufficient. In an ordinary finite difference scheme about 10-20 samples is required per wavelength.

A.5 Time derivative

A standard method is to approximate the spatial derivatives by a spectral method and a finite-difference approach to march in time. Somehow this is an unbalanced scheme leading to finite accuracy in time and indefinite accuracy in space, and so a spectral accuracy in time was introduced to the seismic modeling by Tal-Ezer *et al.* [6]. However, it is considerable simpler to use a finite difference approach for the time derivatives and this is used here, the so-called Euler integration [7] is used. This is faster but not as accurate as spectral methods. For the Biot media the following equations are obtained for the horizontal solid displacement u_x at time $t = k + 1$.

$$\begin{aligned} \frac{\partial u_x(k+\frac{1}{2})}{\partial t} &= \frac{\partial u_x(k-\frac{1}{2})}{\partial t} + \frac{\Delta t}{(m\rho - \rho_f^2)} \left[m \frac{\partial \sigma_{xx}(k)}{\partial x} + m \frac{\partial \sigma_{xz}(k)}{\partial z} - \rho_f \frac{\partial p(k)}{\partial x} \right] \frac{1 - \frac{\Delta t}{2} \frac{\rho \eta}{\kappa}}{1 + \frac{\Delta t}{2} \frac{\rho \eta}{\kappa}} \quad (\text{A26}) \\ u_x(k+1) &= u_x(k-1) + \frac{\partial u_x(k+\frac{1}{2})}{\partial t} \Delta t \quad (\text{A27}) \end{aligned}$$

and a similar set of equations for the solid vertical displacements u_z . The differential horizontal fluid displacements w_x is given by

$$\begin{aligned} \frac{\partial w_x(k+\frac{1}{2})}{\partial t} &= \frac{\partial w_x(k-\frac{1}{2})}{\partial t} + \frac{\Delta t}{(m\rho - \rho_f^2)} \left[\rho_f \frac{\partial \sigma_{xx}(k)}{\partial x} + \rho_f \frac{\partial \sigma_{xz}(k)}{\partial z} - \rho \frac{\partial p(k)}{\partial x} \right] \frac{1 - \frac{\Delta t}{2} \frac{\rho \eta}{\kappa}}{1 + \frac{\Delta t}{2} \frac{\rho \eta}{\kappa}} \\ w_x(k+1) &= w_x(k-1) + \frac{\partial w_x(k+\frac{1}{2})}{\partial t} \Delta t \end{aligned} \quad (\text{A28}) \quad (\text{A29})$$

and a similar set of equations for the differential vertical fluid displacements w_z . The last fraction in Eq. (A26,A28) is due to the viscous forces in the equation of motion which depends on the first derivative.

A.6 Sampling conditions

In order to avoid spatial aliasing it has been found [Kosloff and other empirical studies] that at least two points per wavelength is required in order to obtain that

$$\max(dx, dz) < \frac{1}{2} V_{\min} / f_{\max} . \quad (\text{A30})$$

V_{\min} is the minimum phase velocity for the slowest wave. Thus for the slowest wave in the problem only about two grid points per wavelength is necessary. This is in clear contrast to the sampling criterion for a standard finite difference code, where 10-20 points is required per wavelength. In low velocity zones or in areas with low values of the slow P-wave a dense sampling of the points is required. This poses a problem for a code that is based on a uniform grid.

Based on analytical studies, it has been found [4] for elastic media, and confirmed for Biot media [2], that in order to avoid numerical dispersion the time step Δt must be smaller than

$$\Delta t < 0.2 \min(dx, dz) / V_{\max} . \quad (\text{A31})$$

V_{\min} is the maximum phase velocity for the slowest wave. This criterion, Eq. (A31), requires a small sampling in areas with high velocities, and since the time step must be the same over the whole grid it may force the time step to be extremely small in other regions of the grid.

Both of the above equations should hold for all types of waves. Thus for an elastic media with a low shear velocity Eq. A30 will pose strong limitations on the sampling. For a poroelastic media, where the P-II wave can have a velocity approaching zero it might be impossible to satisfy this criterion.

For accurate modeling of near horizontal and near vertical interfaces it is required to increase the spatial sampling in the direction perpendicular to the interface so that the interface is modeled more precisely. This is further discussed in the examples.

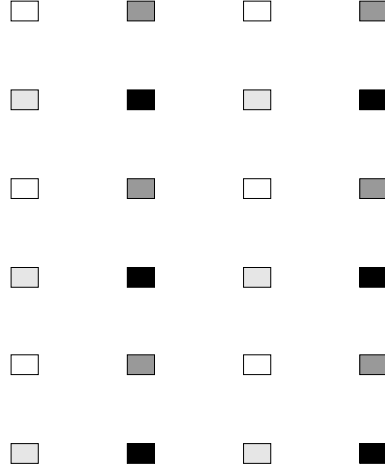


Figure 26: The four subgrids used for the staggered grid formulation. [**grid**]

A.7 Boundary conditions

A main drawback of spectral methods is the requirement of having periodic boundary conditions in space. This causes waves passing one of the grid boundaries to reenter the computational area at the opposite grid boundary. Eventually it will destroy the wavefield under study. In order to avoid this wraparound from one side to the other it is necessary to break the outgoing field at the boundary.

This is still an area of active research. Here, the exponential tapering of the field as suggested by Cerjan [5] is used. Thus the field and its time derivative is tapered by a factor $\exp[-(\beta j)^2]$; $j = 1, \dots, n$ for the n last points of the grid (the sponge layer). Good values are $(n, \beta) = (20, 0.015)$ or $(n, \beta) = (24, 0.0145)$ [according to Turgut Ozdenvar].

It has been found that this type of sponge layer gives good attenuation of the wraparound arrivals. As this tapering acts like an impedance contrast it can give rise to spurious reflections. These are often low frequency and are especially pronounced at the corners of the grid. For these cases lower values of β and larger values of n should be used. Thus when selecting the tapering it is a balance between attenuating the wraparound and avoiding reflections from the sponge layer. It is not always easy to balance the two requirements.

As the field is tapered at each time step the optimal value of the tapering depends also on the time increment. If the time increment is decreased the wave will spend more time in the sponge layer and thus be attenuated more for the same value of β . In order to obtain the same effective attenuation β must thus be reduced.

A.8 Number of FFT blocks

The CPU time is proportional to the number of Fourier transforms required to obtain the second order time derivative. For the three types of media we obtain:

Acoustic: 4 Fourier transforms are needed. These corresponds to the four derivatives of the right hand side of Eq. A1.

Elastic: 8 Fourier transforms are needed. Four to compute the strains and four to compute the derivative of the stresses.

Poroelastic: 12 Fourier transforms are needed. In addition to the ones for elastic media also four transforms are required for the fluid pressure. (The initial formulation [2] required 26 Fourier transforms.

We always base the solution on a staggered grid, as this has proven much more stable, as reported in the literature. The four subgrids used is indicated in Fig. 26, and how the field and material parameters are distributed on these grids is indicated in Table 4. The distribution can easily be determined by first distributing the main field parameter and the field-derivatives and material parameters can then be determined from the field equations.

A.9 Source function

There is no normalization of the source, thus the response from different environmental models cannot be compared. For acoustic media the spatial source function for a source at (x_s, z_s) is:

$$S_p(x, z) = \exp \left[- \left(\frac{x - x_s}{dx} \right)^2 - \left(\frac{z - z_s}{dz} \right)^2 \right] \quad (\text{A32})$$

For elastic and poroelastic media the source function is a vector $(S_x(x, z), S_z(x, z))$:

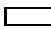



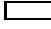


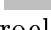
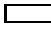



$$S_x(x, z) = \frac{\partial S_p}{\partial x} \quad (\text{A33})$$

$$S_z(x, z) = \frac{\partial S_p}{\partial z} \quad (\text{A34})$$

The temporal source function is a Ricker wavelet with center frequency f_c is applied for $t < 3/f_c$:

$$S_t(t) = \exp \left(-2[tf_c - 1.5]^2 \right) \cos(2\pi[tf_c - 1.5]) \quad (\text{A35})$$

Table 4: Distribution of material and physical parameters on each of the four grids.

	Material	Physical
Acoustic		
	$\frac{1}{\rho c^2}$	p
		
	$\frac{1}{\rho}$	$\frac{\partial p}{\partial z}$
	$\frac{1}{\rho}$	$\frac{\partial p}{\partial x}$
Elastic		
	ρ	u_x
	ρ	u_z
	$\lambda\mu$	$\frac{\partial u_x}{\partial x}, \frac{\partial u_z}{\partial z}$
	μ	$\frac{\partial u_x}{\partial z}, \frac{\partial u_z}{\partial x}$
Poroelastic		
	ρ_f, ρ, m	u_x, w_x
	ρ_f, ρ, m	u_z, w_z
	λ, μ, α, M	$\frac{\partial u_x}{\partial x}, \frac{\partial w_x}{\partial x}, \frac{\partial u_z}{\partial z}, \frac{\partial w_z}{\partial z}, e, \xi, \sigma_{xx}, \sigma_{zz}$
	μ	$\frac{\partial u_x}{\partial z}, \frac{\partial u_z}{\partial x}$

B APPENDIX B: Gas Bubbles in acoustic or elastic media

This section is based on Wood [24], and the expression for sound speed in a two component medium is called Wood's equation.

Assume we have a fraction of gas particles suspended in an acoustic or elastic media. Let ϕ be the volume fraction of gas in the media. Then the density

$$\rho_{\text{eff}} = \phi\rho_g + (1 - \phi)\rho_m, \quad (\text{A36})$$

where ρ_g and ρ_m is the density of the gas and the medium, respectively. Typically $\phi < 1\%$ and thus the effective density is unaffected by the gas.

The shear stiffness is only marginally affected by the gas bubbles in the medium. For moderate void ratios the shear stiffness is assumed constant. Thus the shear speed is also constant.

The effective elasticity modulus E_{eff} is

$$\frac{1}{E_{\text{eff}}} = \frac{\phi}{E_g} + \frac{1 - \phi}{E_m} \quad (\text{A37})$$

where E_g and E_m is the elasticity of the gas and medium, respectively. The sound speed is then given by

$$c = \sqrt{\frac{E_{\text{eff}}}{\rho_{\text{eff}}}} \quad (\text{A38})$$

For the uniform medium $E_m = \rho_m c_m^2$. For the gas we use $c_g^2 = \frac{\partial p}{\partial \rho}$, and for adiabatic gas $p_g \rho_g^{-\gamma} = \text{const}$. This gives $E_g = \gamma P$, where P is the average pressure. For air or hydrogen $\gamma \approx 1.4$.

Just below the ocean surface we have

$\rho_m = 1000 \text{ kg/m}^3$ and $c_m = 1500 \text{ m/s}$, thus $E_m = 2.25 \text{ GPa/m}^2$.

$\rho_g = 1.2 \text{ kg/m}^3$,

$E_g = \gamma P_0 = 1.4 \text{ MPa/m}^2$

The variation of sound speed with void ratio is plotted in Fig. 27(top).

At a depth of 1000 m assuming an average density of $\rho_m = 2000 \text{ kg/m}^3$ and a sound speed of 2000 m/s for a free medium. $E_m = 8 \text{ GPa/m}^2$,

$P = P_0 + z\rho_m g = 0.1 \text{ MPa} + 1000 \cdot 2000 \cdot 10 = 20 \text{ MPa}$ and $E_g = \gamma P = 1.4 \cdot 20 = 30 \text{ MPa}$. The density of the gas is (arbitrarily) assumed $10\rho_{\text{air}} = 12 \text{ kg/m}^3$. The variation of sound speed with void ratio is plotted in Fig. 27(bottom). The effect is somewhat similar to what can be observed with a transversely isotropic media created by a stack of layers with two different media types.

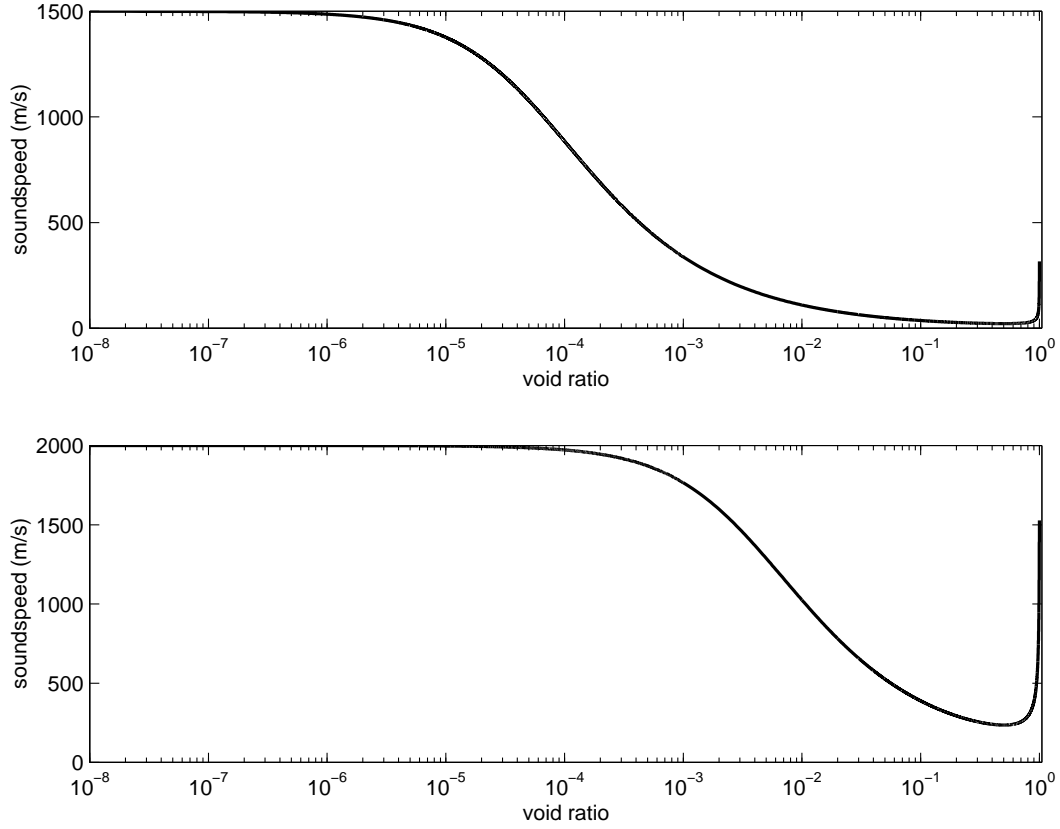


Figure 27: The variation of sound speed with void ratio in a two-component medium. Top: Water and air combined at the top of the ocean. Bottom: A solid and gas combined at 1000 m depth. [**bubble**]

More complicated models of the sound speed variation with void fraction exist. See Deane[25] and Medwin and Clay[1]. It has also been combined with Biot media by Norris [26]

References

- [1] T. Özdenvar and G.A McMehan, “Causes and reduction of numerical artefacts in pseudo-spectral wavefield extrapolation,” *Geophys J. Int.* **126**, 819–828, (1996).
- [2] T. Özdenvar and G.A McMehan “Algorithms for staggered grid computations for poro-elastic, elastic and acoustic, and scalar wave equations,” *Geophysical Prospecting* **45**, 403–420 (1997).
- [3] G. Kneib and C. Kerner “Accurate and efficient seismic modeling in random media,” *Geophysics* **58**, 576–588, (1993).
- [4] D.D. Kosloff and E. Baysal, “Forward modeling by a Fourier method” *Geophysics* **47**, 1402–1412, (1980).
- [5] C. Cerjan, D. Kosloff, R. Kosloff and M. Reshef, “Forward modeling by a Fourier method” *Geophysics* **50**, 1402–1412, (1985).
- [6] H. Tal-Ezer, D. Kosloff, Z. koren, “An accurate scheme for seismic forward modelling” *Geophysical Prospecting* **35**, 479–490, (1986).
- [7] M. Reshef, D. Kosloff, M. Edwards and C. Hsiung, “Three-dimensional acoustic modeling by the Fourier method” *Geophysics* **53**, 1184–1193, (1988).
- [8] M. Reshef, D. Kosloff, M. Edwards and C. Hsiung, “Three-dimensional elastic modeling by the Fourier method” *Geophysics* **53**, 1184–1193, (1988).
- [9] P. Berg, “On forward modelling of seismic waves for exploration of oil and natural gas” Danish center for applied mathematics and mechanics, Technical university of Denmark (1989)
- [10] B. Arntsen, A.G. Nebel and L. Amundsen, “Visco-acoustic finite difference modelling in the frequency domain” *J. Seismic exploration* **7**, 45–64, (1998).
- [11] R.A. Stephen, “A review of finite difference methods for seismo-acoustic problems at the seafloor” *Review of Geophysics*, **26**, 445–458 (1988)
- [12] J.R. Fricke, “Acoustic scattering from elemental Arctic ice features: numerical modeling results” *J. Acoust. Soc. Am.*, **93**, 1784–96 (1993).
- [13] J.A. Fawcett and J.L.T. Grimbergen “Finite difference modelling of scattering in the seabed,” *SACLANTCEN*, SR-256, La Spezia, Italy, (1996).
- [14] M.D. Collins, W.A. Kuperman and W.L. Sigmann “A parabolic equation for poro-elastic media” *J. Acoust. Soc. Am.* **98**, 1645–1656, (1995).
- [15] M. Stern, A. bedford and H.R. Millwater. Wave reflection from a sediment layer with depth-dependent properties. *j. Acoust.Soc. Am.*, 77:1781–1788, 1985.

- [16] J.M. Hovem and J.D. Ingram. Viscous attenuation of sound in saturated sand. *J. Acoust. Soc. Am.*, 66:1807–1812, 1979.
- [17] B. Yavari and A. Bedford. Comparison of numerical calculations of two Biot coefficients with analytical solutions. *J. Acoust. Soc. Am.*, 90:985–990, 1991.
- [18] M.A. Biot. Theory of propagation of elastic waves in a fluid saturated porous solid. *J. Acoust. Soc. Am.*, 28:168–191, 1956.
- [19] R.D. Stoll and T.K. Kan, “Reflection of acoustic waves at a water sediment interface,” *J. Acoust. Soc. Am.*, 70, 149–156, 1981.
- [20] H. Schmidt. SAFARI: Seismo-acoustic fast field algorithm for range independent environments. user’s guide. SR 113, SACLANT ASW Research Centre, La Spezia, Italy, 1987.
- [21] N.C. Dutta and H.Odé, “Seismic reflections from a gas-water contact,” *Geophysics* **48**, 148–162 (1983).
- [22] F.B. Jensen, “On the use of stair steps to approximate bathymetry changes in ocean acoustic models,” *J. Acoust. Soc. Am.* **104**, 1310–1315, (1998).
- [23] A. Sollid “Estimation of P-and S-velocity models from multicomponent seismic data using global optimization and model-based prestack migration”, Statoil Internal Report F&U/980026, 1998.
- [24] A.B. Wood, *A text book on sound*, (Macmillian, New York, 1955).
- [25] G.B. Deane, “Sound generation by breaking waves in the surf zone,” *J. Acoust. Soc. Am.* **102**, 2671–2689, (1997).
- [26] A.N. Norris, “Low-frequency dispersion and attenuation in partially saturated rocks,” *J. Acoust. Soc. Am.* **94**, 359–371, (1993).